Backscatter Communications for 6G

LAKSHMI RAJEEV CHEEKATI AND JIN YAN
MASTER´S THESIS
DEPARTMENT OF ELECTRICAL AND INFORMATION TECHNOLOGY
FACULTY OF ENGINEERING | LTH | LUND UNIVERSITY

Backscatter Communications for 6G

Lakshmi Rajeev Cheekati and Jin Yan
la4541ch-s@student.lu.se, ji5117ya-s@student.lu.se

Department of Electrical and Information Technology
Lund University

Supervisor: Nafiseh Mazloum (Sony) and Ove Edfors (EIT)

Examiner: Buon Kiong Lau (EIT)

September 14, 2022

Printed in Sweden
Tryckeriet i E-huset, Lund

Abstract

The success of future Internet of Things (IoT) depends on, among the other things, developing energy-efficient communication techniques that can enable information exchange among billions of IoT devices with ultra-low/zero power consumption requirements. Ambient backscatter communications is an emerging technology, which utilizes the ambient Radio Frequency (RF) signal as the carrier to reduce the form-factor, and the battery requirements of low-cost small sensor type communication devices. It is, therefore, regarded as a promising technology for massive IoT paradigm, especially for applications with low data-rate requirements. However, ambient backscatter communications face many challenges, such as the presence of strong interference and channel fading. Additionally, these challenges have to be addressed without increasing the complexity and power consumption of the backscatter communication system. Furthermore, the wide-range of prospective backscatter applications means that the performance of ambient backscatter systems have to be studied in a variety of scenarios.

Motivated by this, we study the performance characteristics of ambient backscatter systems using different RF frequencies, data-rates and propagation environments. First, the problem of strong interference is addressed using the well known repetition technique for transmitting the backscatter data. Second, the effects of channel fading are minimized using the scrambling technique. Further, the performance of ambient backscatter systems is studied using a simple quasi-static channel model and a realistic continuous fading channel. The simulations for this purpose are performed using Monte-Carlo simulations in MATLAB. General conclusions are drawn for the relations among different performance metrics, and the effectiveness of the chosen receiver (Rx) structure against channel fading is also evaluated.

Popular Science Summary

Recent developments in wireless communications, and the road towards 6G means that, billions of small communication devices will be used, in a broad range of applications, in the near future. Existing technology for these devices uses complex components, making them costly and consume considerable amounts of energy, as they have to generate their own radio signals. Therefore, it is interesting to explore an alternative technology, in which these small devices can be designed with simple components, and require little to no power to operate. Ambient backscatter technology is one such alternative, in which the devices can communicate using the ambient radio signals, generated from already existing sources like Wi-Fi routers and cellphone towers. This technology can also allow devices to harvest energy from the ambient signals, thereby making them self-sustainable. These features mean that the ambient backscatter devices can operate with a net-zero/ultra-low power consumption.

That said, the ambient backscatter technology is at its infancy, and it needs to overcome many challenges, before it is adopted widely. For instance, the backscatter signals are typically very weak, and they face strong interference from the existing signals in the environment. In addition, backscatter signals are also severely affected by the fading in the channels. It becomes a challenge for the backscatter devices to solve these problems, using simple designs, and very low power consumption. Furthermore, a wide range of future applications mean that the performance of ambient backscatter systems needs to be studied across various environments.

Therefore, in this thesis, we provide simple structures for the backscatter device and the receiver, and we address the above problems using well-known transmission and detection techniques. We also study the performance of ambient backscatter systems across different channels, environments, and frequencies. In addition, we provide an analysis on how the error rates, data rates, and signal coverage of ambient backscatter systems are related to one another in a variety of scenarios.

Acknowledgment

We like to express our gratitude and appreciation for the supervisors Dr. Nafiseh Mazloum and Prof.Ove Edfors for their consistent support and guidance throughout the thesis. We are forever grateful for their patience in leading us in the right direction. The meetings and conversations have been invaluable, without which, this thesis would not have been possible.

We would also like to thank our friends Bharat, Nikhila, Jingxin, Xiaojia, Xiaomeng and Chenyang for cheering us up, and motivating us through hard times. To conclude, we cannot forget to thank our families for all the unconditional support. They firmly supported us with everything they can offer.

Lakshmi Rajeev and Yan Jin

Table of Contents

List of Figures

List of Tables

Acronyms

ADCs Analog to Digital Converters
AmBCSs Ambient Backscatter Communication Systems
ASK Amplitude Shift Keying
AWGN Additive White Gaussian Noise
BBCSs Bistatic Backscatter Communication Systems
BCSs Backscatter Communication Systems
BER Bit Error Rate
DACs Digital to Analog Converters
EM Electro-Magnetic
EPA Extended Pedestrian A
FSK Frequency Shift Keying
INR Interference to Noise Ratio
IoT Internet of Things
LOS Line Of Sight
MBCSs Monostatic Backscatter Communication Systems
ML Maximum-Likelihood
mMTC massive Machine Type Communications
OFDM Orthogonal Frequency-Division Multiplexing
PSK Phase Shift Keying
RF Radio Frequency
RFID Radio-Frequency IDentification
Rx Receiver
SINR Signal to Interference plus Noise Ratio
SIR Signal to Interference Ratio
SNR Signal to Noise Ratio
Tx Transmitter

Chapter 1
Introduction

1.1 Background and Motivation

The 6G wireless communication network is expected to enable immersive communication, and massive IoT, supporting a massive number of connected devices that transmit small amounts of data. Recent forecasts show that massive IoT technology will account for the majority of communication devices in the near future. Therefore, we can foresee a world where, billions of low-cost small-sensor type IoT devices could be deployed in the near future. Using batteries to power these small IoT devices can, however, make them bulky and more expensive, thus creating a necessity for developing IoT devices with zero/ultra-low power consumption. Existing low-power IoT solutions such as Narrow Band IoT [1], massive Machine Type Communications (mMTC) [2], and RedCap [3] may be not sufficient to meet the future demands, due to their conventional designs and the use of analog components, which require considerable power consumption. Therefore, it is interesting to explore other emerging technologies with the potential of realizing zero/ultra-low power requirements of future massive IoT applications, and also meeting the standards of 3GPP. Backscatter communications is one such technology, that has recently gained attention as a promising alternative for existing IoT solutions.

Backscatter Communication Systems (BCSs) allow a device to communicate using the RF signals originating from an external source instead of generating them itself [6], [7]. Ambient Backscatter Communication Systems (AmBCSs) is a class of backscatter technology in which, as the name suggests, ambient RF signals are utilized for communications. Recently, AmBCSs are gaining importance, since the ubiquitous presence of different wireless networks can provide a reliable source of Electro-Magnetic (EM) waves, even at inaccessible locations. The main advantage of implementing backscatter technology is that it eliminates the need for power-intensive RF components such as mixers, Analog to Digital Converters (ADCs) and Digital to Analog Converters (DACs), thus greatly reducing device energy consumption. Therefore, this technology is considered effective in addressing costs and energy-efficiency problems for low-power communications systems such as small-sensor type IoT applications. Backscatter technology is already used in many practical applications, such as Radio-Frequency IDentification (RFID), packaging and logistics, tracking devices, and low-cost sensor networks [8]. Despite high expectations, studies for understanding the true potential of backscatter

technology, especially AmBCSs, are still in their emerging phase. Therefore, in this thesis work, we aim to study the AmBCSs performance in terms of Bit Error Rate (BER), data-rate, and coverage, and analyze the relation among them for different scenarios.

1.2 Methodology

In this thesis, we provide an overview of AmBCSs performance, using a simple backscatter device and Receiver (Rx) structure. For our analysis, we use two types of channel models: a simple quasi-static channel model and a realistic continuous fading channel model. These simple models allow us to perform quick simulations across different propagation environments, and RF frequencies. We also study two different modulation techniques for the backscatter device, to address the interference and channel fading at the Rx, and we discuss the limitations of our Rx structure under realistic fading conditions. We use Monte-Carlo simulations in MATLAB for performing our analysis in this thesis.

1.3 Contributions

As we will see later, interference is one of the key challenges for AmBCSs, and we use the well known repetition technique for making the Rx less susceptible to interference. We also study a new waveform for modulating the data at the backscatter device, which can reduce the effect of channel fading at the Rx and also simplify the detection process considerably. We then analyze the AmBCSs performance using the BER, data-rate, and coverage, which are some of the important metrics for evaluating a communication system. We analyze the AmBCSs performance using these metrics under different channel models, propagation environments and RF frequencies, and also evaluate the relations among them. Additionally, the requirements and possibilities for the BER, data-rate, and coverage of AmBCSs may vary significantly, due to the wide-range of potential applications and use-case scenarios. Therefore, we use simple geographical illustrations that analyzes AmBCSs coverage for different BERs and data-rates across different propagation environments and RF frequencies.

1.4 Thesis Organization

The organization of this thesis is as follows:

In Chapter 2, we provide a general overview of different backscatter system types and also discuss the characteristics of selected state-of-the-art AmBCSs designs. In Chapter 3, we introduce an analytical model for AmBCSs, based on simplified assumptions, and discuss the characteristics of transmission and detection schemes used in our system model. In Chapter 4, we discuss the simulation results and analyze performance of AmBCSs across different propagation environments, and for two different channel models. We also study the relations among BER, data-rate and coverage area of AmBCSs, and discuss the trade-offs involved

in obtaining a balance among them to fulfill a certain requirement. Finally, we conclude this thesis by summarizing the main outcomes, and outlining the directions for future work in Chapter 5.

Chapter 2
Background

Backscatter Communication Systems (BCSs) have many fundamental differences to conventional wireless communications systems. It is therefore important to have a good understanding of the BCSs' characteristics, as well as their capabilities and limitations. In Section 2.1, we provide an overview of BCSs, and describe the principle behind the data modulation of BCSs. In Section 2.2, we describe the classification of BCSs, based on their architecture, in more detail. Later, in Section 2.3, we outline some of the latest advancements in AmBCSs, and discuss their performance characteristics and limitations.

2.1 Overview

The basics of backscatter communications are conceptually similar to those of an old communication technique using a signaling instrument called the heliograph, shown in Figure 2.1. A heliograph is a device that communicates by reflecting the sunlight, using mirrors [4]. An operator can control the presence of the reflected light by flipping a mirror, and can signal a remote target using, e.g., Morse code. Similarly, a backscatter device reflects an incoming RF source signal in a controlled way, resulting in a backscatter signal that can be picked up by a Rx. In this sense, backscatter communication can be viewed as a technique that allows a device to communicate without the need to generate its own RF signal.

The first known use of backscatter techniques using radio waves dates back to World War II [9], when German radar operators used passive backscatter radio links for identifying friendly Luftwaffe aircraft. The pilots of German fighter squadrons, when being illuminated by German radars, would all perform a foreknown maneuver. The German radar operators would then follow the changes in the blips on their radar screens and identify them as friendly aircraft. However, using backscatter techniques for 'wireless communications' was first proposed by Harry Stockman in 1948 [10], by providing a theoretical foundation for RFID technology. The RFID technology has since gained prominence, and it is currently used in many applications, such as inventory management, device tracking, and access control.

The operational principle behind almost all existing BCSs is based on the above principles. The backscatter device in a BCS reflects, and simultaneously modulates an incident RF signal to transmit its own data. This reflection and

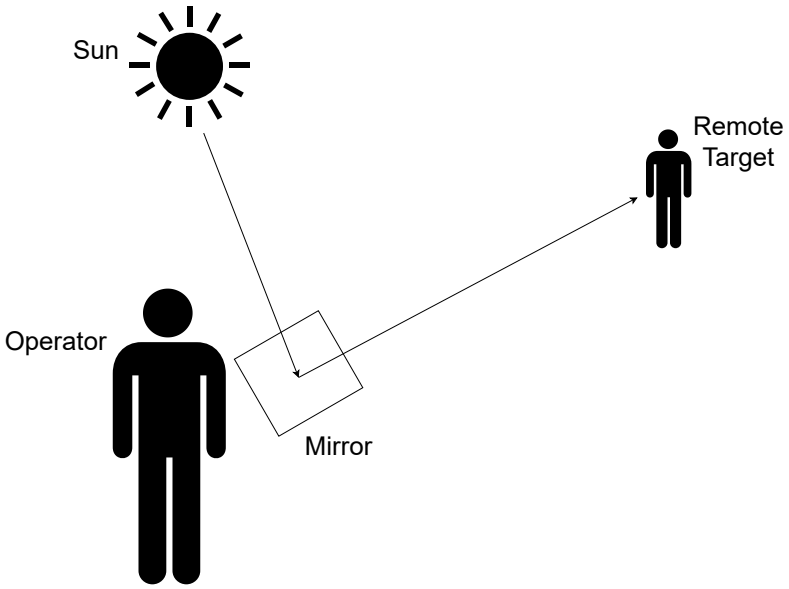

Figure 2.1: The Heliograph: an optical communication technique using sunlight.

data modulation, at the backscatter device are typically achieved by exploiting "impedance mismatch", as described below.

Let us consider a backscatter device with a load-impedance Z_L, and antenna-impedance Z_a as shown in Figure 2.2. The backscatter device can now modulate its data by manipulating the mismatch between Z_L and Z_a, and switching between 'non-reflecting', and 'reflecting' states [27]. In its reflecting state, the backscatter device can completely absorb an incident RF wave by setting $Z_L = Z_a^*$. On the other hand, setting the load impedance of backscatter device as $Z_L = 0$ results in a perfect wave reflection, forming its 'reflecting state'. The backscatter device can thus implement a binary modulation scheme, by switching between the above two states to transmit bits 1 and 0, respectively. In practice, the switching between these states in the backscatter device is implemented using RF switches [12], as shown in Figure 2.2.

The reflection coefficient (γ) of the backscatter device antenna is given as [27]

$$\gamma = \frac{Z_L - Z_a^*}{Z_L + Z_a}, \tag{2.1}$$

and $|\gamma|$ represents the ratio of the reflected wave amplitude to that of incident wave. The corresponding values of $|\gamma|$ for the above-mentioned binary modulation scheme are $|\gamma| = 0$ for the 'non-reflecting' state and $|\gamma| = 1$ for the 'reflecting' state. It is even possible to get higher modulation orders by tuning Z_L such that

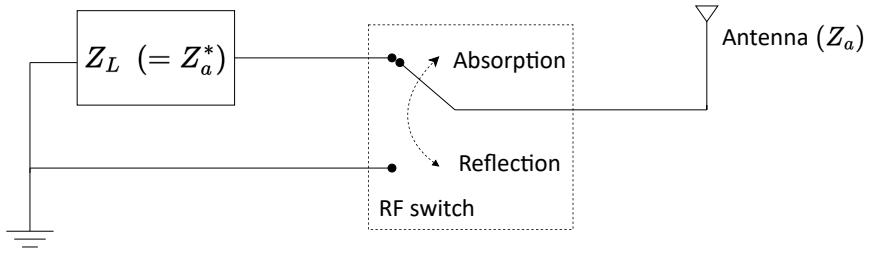

Figure 2.2: Implementation of impedance matching for modulating backscatter data.

multiple values for γ can be achieved (e.g., with phase modulation such that, different phases that correspond to the same $|\gamma|$ value are obtained).

2.2 Classification of Backscatter Communication Systems

BCSs can be classified differently, depending on the type of RF source signals, modulation schemes, architecture, and use-case scenarios. For the scope of this work, we limit ourselves to discussing the classification of BCSs based on their architecture.

Before proceeding to such a classification, let us discuss the difference between BCSs and conventional wireless communication systems. Simple block diagrams for a comparison between a BCS and a conventional wireless communication system are shown in Figure 2.3. A conventional wireless communication system, as shown in Figure 2.3a, consists of two devices namely, a Transmitter (Tx), and a Rx. These two devices communicate through a single wireless channel, denoted as 'communication link'. The conventional Tx generates its own RF carrier signal, required to modulate the baseband information signal. Unlike conventional wireless communication systems, a typical BCS consists of three main devices, namely, an RF signal source, a backscatter device, and an Rx, as shown in Figure 2.3b. In case of BCSs, the carrier signal is sourced from the 'RF source', instead of generating it within the backscatter device. With this, the communication channel in the BCS is split into two links, i.e., 'forward link', and 'backscatter link'. The forward link refers to the wireless channel between the RF source and the backscatter device, and the backscatter link is the wireless channel between the backscatter device and the Rx. A drawback of BCSs is that the Rx also receives the RF signal from the RF source through a third wireless channel, shown as the 'interference link' in the Figure 2.3b, which acts as an interference at the Rx.

Now that the basic distinction between BCSs and conventional wireless communication systems is outlined, let us discuss the classification of BCSs based on their architectures. The BCSs are typically classified into three major types, which are,

- Monostatic Backscatter Communication Systems (MBCSs)

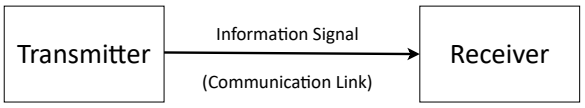

(a) Conventional Wireless Communication System

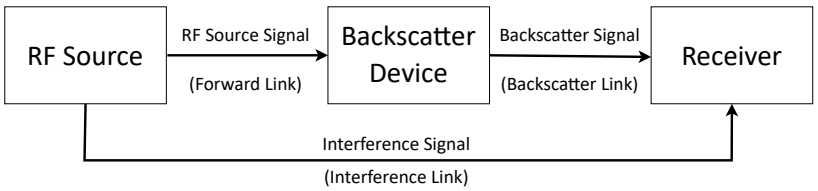

(b) Backscatter Communication System

Figure 2.3: Simple block diagrams of Conventional vs Backscatter Communication Systems. Note: The term 'link' in this figure denotes a wireless channel.

- Bistatic Backscatter Communication Systems (BBCSs)
- Ambient Backscatter Communication Systems (AmBCSs)

We describe each of these types in the following subsections, in more detail.

2.2.1 Monostatic Backscatter Communication Systems (MBCSs)

The key characteristic of MBCSs is the incorporation of the RF source and the backscatter receiver into a single device, forming a transceiver, as shown in Figure 2.4. The RF source in the MBCS transceiver generates the RF source signal, commonly referred to as 'excitation signal', that is required to activate the backscatter device. The backscatter device then transmits its data by modulating and reflecting the backscatter signal to the transceiver.

Since the RF source and Rx are in the same device, MBCSs suffers from round-trip path loss [13]. It is well known that the loss of signal power increases with propagation distance. Therefore, the co-existence of the RF source and the Rx in MBCSs also means that, both the forward link and backscatter link distances are simultaneously increased when the backscatter device is moved away from the transceiver. This leads to the doubly near-far problem in MBCSs [14]. The MBCSs also face self-interference, where the unmodulated excitation signal dominates the incoming backscatter signal by several orders of magnitude [9]. The backscatter signal quality in MBCSs is therefore significantly reduced due to the above factors, resulting in very limited coverage. However, regardless of these limitations, MBCSs are widely used in a number of applications. A common and extensive use of MBCSs can be found in the form of RFID tags, which are used in banking, logistics,

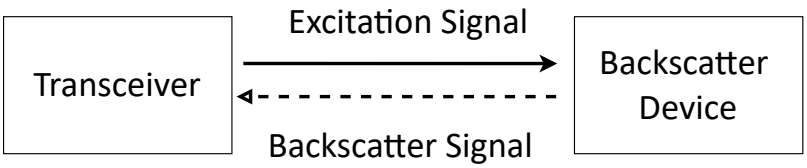

Figure 2.4: Block diagram for MBCSs architecture where the RF source and the Rx are placed in the same device.

and warehousing applications. Despite the wide range of use-cases, one common drawback among all MBCSs applications is the severe limitation in the coverage, which is often limited to up to a meter or so. The above-mentioned challenges of the MBCS architecture can be addressed by instead employing a bistatic architecture, as discussed in the following subsection.

2.2.2 Bistatic Backscatter Communication Systems (BBCSs)

As the name suggests, the "bistatic" architecture means placing the RF source and the Rx at different locations. The main difference between the MBCS and BBCS configurations is the breakup of the previously mentioned MBCS transceiver into two separate devices. A general block diagram of a BBCS architecture is presented in Figure 2.5, showing the RF source, Rx, and backscatter device, placed in different locations.

The RF source in BBCSs is commonly referred to as the 'carrier emitter', which transmits the excitation signal in the form of an unmodulated carrier signal. Typically, these carrier emitters are entirely dedicated for backscatter operations. The fundamental operation of BBCSs is similar to that of MBCSs, where the backscatter device modulates and backscatters the excitation signal originating from the RF source. This backscatter signal is then picked up by the Rx, located in a different location than the RF source. Additionally, the bistatic configuration also faces direct interference at the Rx from the unmodulated carrier signals, as shown in Figure 2.5.

The ability of the bistatic configuration to separate the Rx from the RF source addresses the major issues faced by MBCSs, such as avoiding the round-trip path loss. Since the RF source and the Rx in BBCS are no longer co-located, spatial flexibility can be achieved by placing one of them in an optimal location. For instance, placing the carrier emitters closer to backscatter devices resolves the doubly near-far problem faced by the MBCSs [14]. Another approach is to use a centralized Rx and place multiple carrier emitters around backscatter devices, so that the overall field coverage can be improved [15].

The above-mentioned characteristics of BBCSs enable their usage in appli-

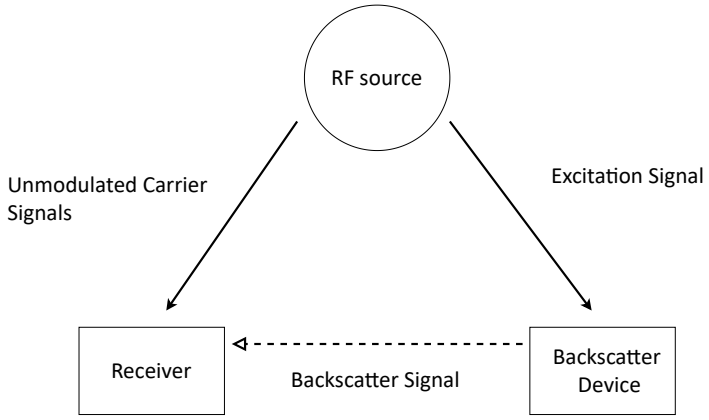

Figure 2.5: Bistatic Backscatter Communication System architecture with the RF source, and the Rx, placed in different locations

cations with much greater coverage than those of MBCSs. For example, recent backscatter technologies like LongRange(LoRa) [16] and Lorea [17] use the BBCS architecture to support longer range communications compared to MBCSs. However, the application of BBCSs comes with certain disadvantages. One such disadvantage is the need to deploy multiple carrier emitters, increasing the amount of hardware required. Furthermore, we have already mentioned that these carrier emitters are dedicated for backscatter operations. This means that the BBCSs require dedicated RF spectrum resources, which is another disadvantage. Moreover, using dedicated RF resources removes the ability of spectrum sharing and limits the possibility of integrating BBCSs with conventional communication technologies. However, these limitations of BBCSs can be addressed by replacing the dedicated carrier emitters of BBCSs with existing ambient RF sources, which is discussed in the next subsection.

2.2.3 Ambient Backscatter Communication Systems (AmBCSs)

As the term 'ambient' suggests, AmBCSs source their RF signals from existing RF sources, e.g., Bluetooth, Wi-Fi access points, base stations, or TV towers, instead of using dedicated carrier emitters as in the BBCSs. Intuitively, the 'heliograph' analogy in Section 2.1 can be related more specifically to the AmBCSs. This is because, the heliograph operator makes use of ambient sunlight for communicating, instead of using any dedicated light source like, for instance, light bulb or torch. This is similar to what is achieved with AmBCSs by using ambient RF sources. The architecture of a typical AmBCS consists of three major components, namely,

'ambient RF source', 'backscatter device', and 'Rx', as shown in Figure 2.6. Note that the ambient RF source in this figure is different from the dedicated 'carrier emitter' used in BBCSs.

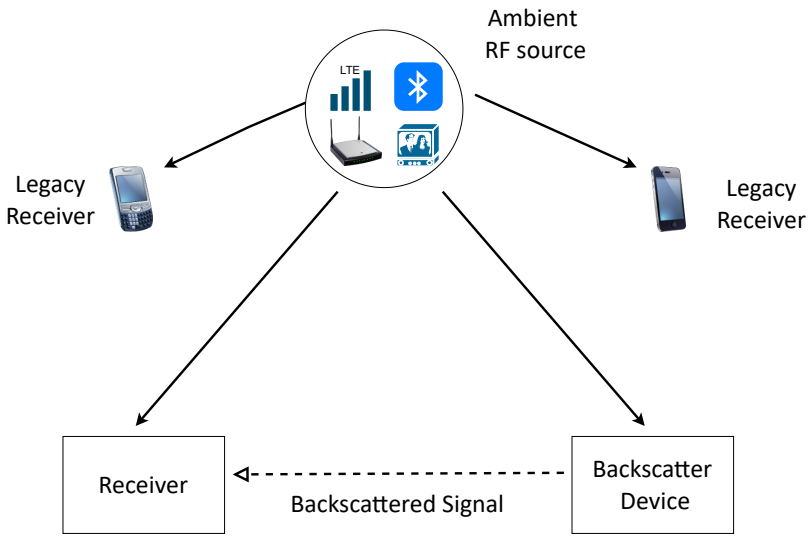

Figure 2.6: Ambient backscatter system architecture.

AmBCSs address the drawbacks of BBCSs by making use of already existing RF signals and eliminating the need for both dedicated carrier emitters and the usage of additional frequency spectrum. However, AmBCSs also have their own drawbacks as follows:

- AmBCSs have no control over the presence, or strength, of ambient RF signals. Hence, they have to operate in the presence of unknown and random ambient RF signals.
- Another drawback of AmBCSs is the ambient RF signal acting as direct interference at the Rx, which needs to be taken into account. Unlike in BBCSs, where the Rx typically has the knowledge of the unmodulated carrier signals, the Rx in AmBCSs has no knowledge of the interference signal characteristics, and hence it is difficult for the Rx to cancel it.

Despite the above-mentioned hurdles, AmBCSs are still viewed as a promising technology for future IoT applications [21]–[25]. The concept of using ambient signals holds some interesting possibilities: By sharing the same RF resources with traditional communication systems, AmBCSs have the possibility of reusing existing infrastructure and connecting backscatter devices to larger networks, like the Internet [21]. AmBCSs are also expected to have the potential to directly

generate conventional signal transmissions, that can be decoded by any existing wireless device [23]. However, the practical applications of AmBCSs are still in their emerging phase, with various proof-of-concepts demonstrating the feasibility of AmBCSs, using prototypes and simulation models.

So far in this section, we have discussed the characteristics of each backscatter system architecture, and outlined their benefits and drawbacks. However, it is worth mentioning here that both MBCSs and BBCSs are widely studied for improving their designs and performances, compared to AmBCSs. This lack of extensive studies on AmBCSs, combined with the previously mentioned potentials of AmBCSs, prompts us to focus our remaining work mainly on AmBCSs. In the following section, we briefly discuss some existing designs of AmBCSs, and outline their performance characteristics.

2.3 State of the Art

One of the first successful prototypes for AmBCS is proposed in [18], leveraging background TV transmissions. Another successful prototype is a FM backscatter system [20], which proposed the use of ambient FM radio signals. The possibility of using ambient Wi-Fi signals was also explored recently, by modulating the Wi-Fi channel information with backscatter data in [21], and by embedding the backscatter data on standard 802.11b packets in [22, 23]. The interoperability of backscatter systems between different RF technologies was also studied recently, by converting Wi-Fi packets into Bluetooth transmissions [25, 26].

In order to maintain simplicity in the backscatter device design, the backscatter signal modulation in AmBCSs is typically confined to binary schemes, such as Amplitude Shift Keying (ASK) in [18, 22], Phase Shift Keying (PSK) in [20], and Frequency Shift Keying (FSK) in [20, 25]. However, efforts have been made for using higher level modulations in AmBCSs to overcome the low spectrum efficiency and the low data rate of binary modulation schemes. For instance, some recent studies have explored the possibility of implementing M-ary QAM, e.g., 16-QAM [32] and 32-QAM [33], as well as N-PSK, e.g., 4-PSK and 16-PSK [24] at the backscatter devices.

The performance characteristics of the above-mentioned works, however, vary greatly. There are a few surveys like [27, 28], compiling recent AmBCSs designs and discussing their advantages and disadvantages. However, these surveys only discuss the AmBCSs designs individually, and do not compare them with one another. This is due to the vast differences in their design approaches, making it difficult to have a fair comparison. Table 2.1 summarizes the performance characteristics of some existing AmBCSs designs, on the basis of coverage, bit-rate and BER. We can see in this table that the coverage and data-rates of these designs are different to one another. This is because of different and incomparable experimental setups, RF signal choices, modulation schemes, and assumptions used in these AmBCSs designs.

To the best of our knowledge, current studies about AmBCSs mainly provide hardware prototypes and practical measurement results. Moreover, analysis on the relations among different performance characteristics of AmBCSs is not avail-

Design	Coverage	Bit Rate	BER
LoRa[16]	2.8 km	37.5 kbps	-
LoRea[17]	3.4 km	197 kbps	-
TV backscatter[18]	2.5 ft (outdoor) /1.5 ft (indoor)	1 kbps	10^{-2}
FM backscatter[20]	18.3 m	3.2 kbps	-
Back-Fi[24]	1m/5 m	5 Mbps/1 Mbps	-
Wi-Fi backscatter[21]	$2.2 - 3$ m	$5 - 20$ kbps	-
HitchHike[22]	34 m	300 kbps	-

Table 2.1: Performance comparison of AmBCS designs

able in these works. It is also worth mentioning that almost none of the designs in Table 2.1 have been analyzed with respect to their performance in BER. There are also studies such as [34, 35, 36], which investigate the detection schemes and BER for AmBCSs, and these studies are all based on Signal to Noise Ratio (SNR) at the Rx. However, as mentioned in the previous section, interference has significant influence on AmBCS performance, and it cannot be ignored. Therefore, in this thesis, we study the AmBCS performance in the presence of interference, and discuss the relations among different performance characteristics through simulations. In the next chapter, we start by discussing AmBCSs' system model along with the transmission and detection schemes, taking interference into account. We also formulate necessary analytical expressions needed for our analysis.

Chapter 3

System Model and Signal Design

In this chapter, we present the AmBCSs' system model, used for analyzing the AmBCS performance, along with the necessary analytical expressions. We also describe each component in this system model, and discuss their characteristics in more detail. This chapter starts by deriving the overall expression for the received signal using our system model in Section 3.1. Further, in Section 3.2, we discuss the typical sources for the ambient RF signal, and describe its modeling for our analysis. In Section 3.3, we discuss the waveforms for two different transmission schemes at the backscatter device, for increasing the robustness of the Rx against the interference and channel fading effects. Here, we also describe the implementation of these transmission schemes using a simple backscatter device structure. In Section 3.4, we describe the detection scheme at the Rx, and discuss its implementation using simple block diagrams. Later in Section 3.5, we set up the link budget for AmBCSs, and derive the expressions for backscatter signal quality, in the presence of interference.

3.1 System Model

In this section, we describe the system model used for analyzing AmBCS performance and derive the overall analytical expression for the signal received at the Rx. The system model for an AmBCS is presented in Figure 3.1, where the ambient RF source, backscatter device, and Rx are shown in their respective blocks. The wireless channels between these components are shown as the forward, backscatter, and interference links, and the channel coefficients for these links are denoted as $h_f(n)$, $h_b(n)$, and $h_i(n)$, respectively. The signal components corresponding to each link are also shown in this figure.

Let us now derive the expressions for the signal components step by step, and find the overall expression for the received signal. Let us consider that the ambient RF source transmits a band-limted analog RF signal, and denote it in discrete-time representation as $s(n)$. The RF signal component reaching the backscatter device can be written as

$$s_{in}(n) = s(n) * h_f(n), \tag{3.1}$$

where '$*$' represents convolution. Assuming that the backscatter device modulates its data using impedance matching, described in Section 2.1, the backscatter signal

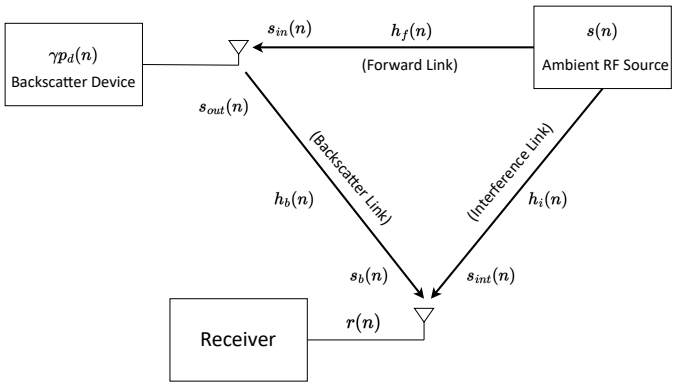

Figure 3.1: AmBCS system model with a discrete-time representation of its signal components.

reflected from the backscatter device can be written as

$$s_{out}(n) = \gamma p_d(n) s_{in}(n), \tag{3.2}$$

where $\gamma p_d(n)$ is the modulation signal generated within the backscatter device, and $d \in \{0, 1\}$ is the backscatter data. The backscatter device generates $\gamma p_d(n)$ using one of the two binary transmission schemes, discussed in Section 3.3 in more detail. The noise in the backscatter device has negligible contribution at the Rx side, compared to the Rx' own noise. Therefore, here, we ignore the noise generated within the backscatter device. Similar to (3.1), the expression for backscatter signal component, reaching the Rx is

$$s_b(n) = s_{out}(n) * h_b(n), \tag{3.3}$$

which can be re-expressed using (3.1) and (3.2) as

$$s_b(n) = (\gamma p_d(n)(s(n) * h_f(n))) * h_b(n). \tag{3.4}$$

Similarly, the expression for the interference component at the Rx is

$$s_{int}(n) = s(n) * h_i(n). \tag{3.5}$$

The overall received signal at the Rx is the summation of the signals received from the backscatter link and the interference link. Using (3.4) and (3.5), the expression for the overall received signal $r(n)$ at the Rx becomes,

$$r(n) = \underbrace{s(n) * h_i(n)}_{\text{interference}} + \underbrace{(\gamma p_d(n)(s(n) * h_f(n))) * h_b(n)}_{\text{backscatter component}} + w(n), \tag{3.6}$$

where $w(n)$ is the complex Additive White Gaussian Noise (AWGN) at the receiver. Note that all backscatter applications mentioned in the previous chapters expect the devices to be either stationary, or slow-moving. Therefore, we can assume that the channels in backscatter systems stay fixed for a considerable duration. Here, assuming the channels are fixed during each bit transmission, i.e., 'Quasi-Static', the channel coefficients h_f, h_b, and h_i become flat-fading. Therefore, the above equation can be further simplified and rearranged as,

$$r(n) = (\alpha(n) + \beta(n))s(n) + w(n), \tag{3.7}$$

where $\alpha(n) = h_i(n)$ and $\beta(n) = \gamma p_d(n) h_f(n) h_b(n)$.

We have now derived the overall expression of the signal received at the Rx, using an ambient RF signal $s(n)$, and by simply denoting the modulated signal at the backscatter device as $\gamma p_d(n)$. Let us briefly discuss the ambient RF signal $s(n)$ in the next section, and then study the modulated signal $\gamma p_d(n)$ in more detail later.

3.2 Ambient RF Source

Depending on the communication environment, the ambient RF signals may come from a variety of sources. We know that the majority of existing wireless communication systems such as, Bluetooth, Wi-Fi, cellular networks, and digital television are typically based on Orthogonal Frequency-Division Multiplexing (OFDM). Typically, the baseband representation of an OFDM signal has a distribution equivalent to a band-limited white Gaussian noise. An OFDM signal is an orthogonal transform (DFT) of independent data points on the subcarriers, which makes it having a white Gaussian noise distribution, except for the cyclic correlation introduced by the cyclic prefix. Given the ubiquitous presence of these OFDM based wireless communication systems, it is logical to consider that the ambient RF signals for AmBCSs are typically OFDM signals. Therefore, if we can ignore the cyclic prefix in this study for simplicity, the ambient RF signal $s(n)$ used in the previous section can be modeled as a zero-mean complex Gaussian random variable with zero-mean and a variance of σ_s^2, i.e., $s(n) \sim \mathcal{CN}(0, \sigma_s^2)$. Such modeling generalizes our system model so that the conclusions drawn from this study can be applied across other RF sources that show Gaussian characteristics.

3.3 Transmission Scheme

The purpose of the backscatter device is to modulate a sequence of data bits, and transmit them using the reflected RF signal. The transmission scheme of most AmBCSs is based on switching the antenna load between 'non-reflecting' and 'reflecting' states, as discussed in Section 2.1. However, backscatter signals face the challenges such as, strong interference, and channel fading. Therefore, the modulation techniques at the backscatter device need to possess the characteristics required to address these challenges. In this section, we discuss two modulation techniques that are capable of addressing the interference at the Rx, and one of these techniques can also mitigate the channel fading problem in the AmBCSs.

The dual path losses involved in backscatter communications, and the presence of strong interference, make it difficult for the Rx to detect the weak backscatter signals. Therefore, the backscatter device needs to adopt modulation technique, that can help gather enough signal energy at the Rx for extracting the backscatter data. This is typically achieved using the well known 'Repetition' technique. In this technique, the backscatter data-rates are lowered by transmitting the bits over longer duration, thus increasing the backscatter signal energy. In terms of a discrete-time model, repetition involves transmitting each backscatter bit repeatedly, over multiple samples of an ambient RF signal.

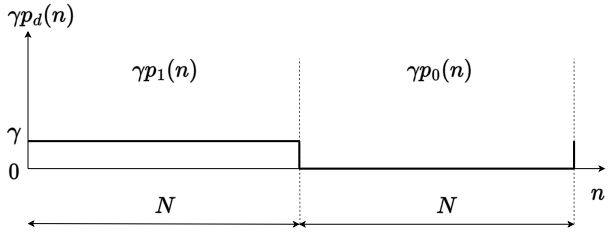

(a) Waveform for repetition technique.

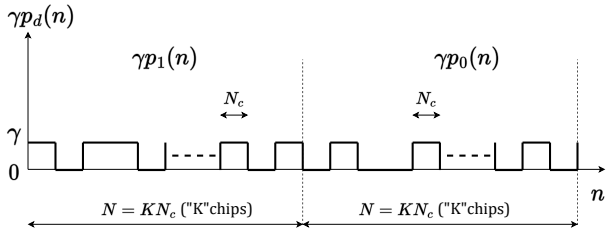

(b) Waveform for scrambling technique.

Figure 3.2: Backscatter signal waveforms for the repetition and scrambling techniques.

The backscatter signal waveform, modulated using the repetition technique, is shown in Figure 3.2a. In this figure, each backscatter bit is shown to be transmitted over N samples of an ambient RF signal. This parameter N, therefore, represents the number of ambient RF signal samples required for transmitting each backscatter bit, and is defined as the repetition factor. Given that the backscatter device modulates its data using a high enough repetition factor, the Rx can gather sufficient backscatter signal energy and detect the backscatter data, even in the presence of strong interference.

On the other hand, channel fading causes distortions in the transmitted signals. This makes it difficult for the Rx to differentiate between different symbols of rep-

etition technique, which are separated over longer duration. Moreover, AmBCSs may not have the possibility to transmit additional signals (e.g., pilot signals) for estimating the channel, due to the simplicity and ultra-low power requirements of the backscatter device. Therefore, when designing the backscatter signals, we need to address channel fading through the modulation technique.

Scrambling is one such technique for addressing the channel fading problem using a simple Rx structure. This technique allows the Rx to differentiate between the relative changes between adjacent chips, which are located much closer in time, compared to the longer backscatter bit duration. Thus, the negative influence of channel fading can be significantly reduced using scrambling, as it is more likely for the channel to stay constant over a shorter chip duration, compared to the entire bit duration. Scrambling involves mapping the data bits '0' and '1' to different scrambling sequences, creating pulse sequences with increased signal bandwidths. The scrambling sequences implemented in this work have equal number of 0's and 1's in them, a characteristic which later has advantages at the Rx.

Figure 3.2b shows a modulated backscatter signal waveform using the scrambling technique. In this figure, it is shown that each backscatter symbol is scrambled using a binary spreading code, consisting of K elements (or chips), with a chip duration of N_c ambient RF signal samples.

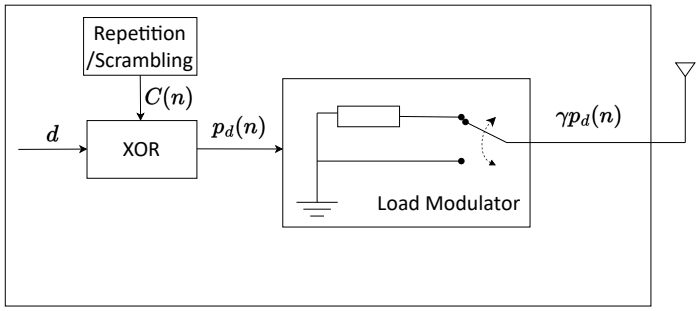

Figure 3.3: Block diagram for implementing the repetition/scrambling transmission scheme at the backscatter device.

Let us now discuss the implementation of the transmission schemes, using a simple block diagram of the backscatter device. Figure 3.3 shows a simple way of implementing the repetition/scrambling technique at the backscatter device for each data bit d. The figure consists of a repetition/scrambling block, which generates a binary pulse sequence $C(n)$, similar to Figure 3.2a when repetition is implemented, and 3.2b when scrambling is implemented. The modulation of the data bit d, using the pulse sequence $C(n)$ is performed using an XOR operation, creating a modulated pulse sequence $p_d(n)$. This modulated sequence $p_d(n)$ is then fed to the RF switch, which uses it as an input to toggle between 'non-reflecting' and 'reflecting' states of the load modulator circuit, thus generating the modulated backscatter signal $\gamma p_d(n)$. This completes the transmission cycle for the data bit d, and the entire process is repeated for each bit in the backscatter device data stream. Now that we have described the repetition and scrambling techniques for

addressing interference and channel fading, respectively, let us proceed to the next section and discuss the signal detection at the Rx for these techniques.

3.4 Detection Scheme

The overall received signal $r(n)$ at the Rx is a combination of interference, backscatter, and noise components as described in (3.7), i.e.,

$$r(n) = (\alpha(n) + \beta(n))s(n) + w(n),$$

where $\alpha(n) = h_i(n)$ and $\beta(n) = \gamma p_d(n) h_f(n) h_b(n)$. The purpose of the Rx is to extract the backscatter data from the signal $r(n)$ in the presence of interference and Rx internal noise. In this section, we describe the mechanism implemented by the Rx to serve this purpose using a simplified description. Here, we start with the assumption of Quasi-Static nature of the channels, because of which, the following description leads to Maximum-Likelihood (ML) detection in the end. Later, we analyze the effectiveness of this Rx mechanism in tolerating the channel fading within the bit duration, in the following chapter.

As mentioned earlier, AmBCSs have to operate in the presence of unknown and random ambient RF signals. This means that AmBCSs cannot use the phase information of the received signal, leaving the option of using the received signal energy for detecting the backscatter data. Therefore, the first step in a Rx for extracting backscatter data, is to measure the energy of the received signal. Now, let us start with considering that the backscatter device transmits its data using the repetition technique, and briefly discuss the challenges of its corresponding detection scheme. In this case, the Rx has the option to detect the transmitted data bit, using the relative difference between the received signal energy of each bit duration. However, implementing a detection scheme for the repetition technique comes with the following challenges:

- Such a detection is based on comparing the signal energies across bit duration. This means that the Rx needs to find a pre-defined threshold for comparing the signal energy, which can increase the complexity of the Rx structure.
- The necessity for a pre-defined threshold also means that, the backscatter device is now required to transmit additional signals, for instance pilot signals, for the Rx to calculate the threshold. However, this is not desirable in view of the simplicity and energy efficiency requirements of the backscatter device designs.
- Lastly, the comparison of changes in the signal energy is performed over 'much longer' bit duration. Although this has no significance for a Quasi-static channel, such a Rx can suffer significantly when the channel fades continuously.

On the other hand, the detection scheme for the scrambling technique can be implemented in a simple way, bypassing the above challenges. Let us now consider that the backscatter device transmits its data using the scrambling technique,

and discuss the detection scheme for this case, implemented using simple steps as shown in Figure 3.4. As described earlier, each bit using the scrambling technique is transmitted using a binary pulse sequence with K chips, each with duration of N_c samples. This means that the presence, or absence of the backscatter signal component at the Rx changes for every N_c samples (or) chip duration. The Rx can exploit this for extracting the backscatter data, by detecting the relative changes in the signal energy for each chip duration. This is done by first calculating the received signal energy in the following way:

$$R(k) = \sum_{n=kN_c}^{(k+1)N_c} |r(n)|^2, \ 0 \leq k \leq K-1, \tag{3.8}$$

where $R(k)$ is the total received signal energy for each chip duration, and k is the chip index inside each bit transmission. The Rx can now detect the relative changes in the signal energy between each chip duration, using the sequence $R(k)$.

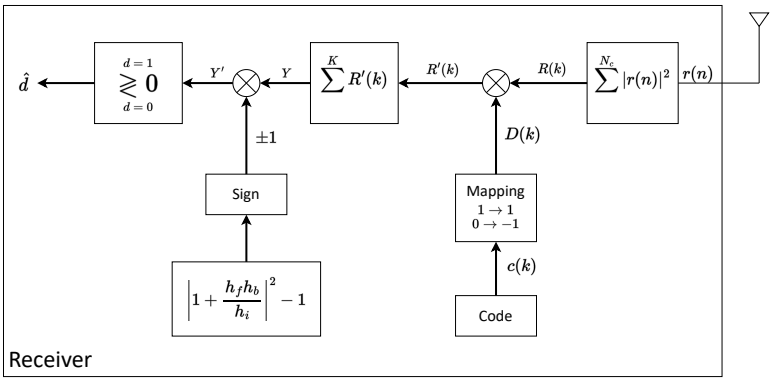

Figure 3.4: Block diagram for implementing ML detection in the Rx.

Earlier, we mentioned that the scrambling sequence has an equal number of 1's and 0's, a characteristic which is advantageous for detection. The Rx makes use of this characteristic, and compares the signal energy corresponding to the "1's" in the scrambling sequence, with that of the "0's". Since we have equal number of 1's and 0's in the scrambling sequence, the threshold for such comparison becomes zero for all cases. This eliminates the need for calculating any pre-defined threshold for scrambling, thus significantly simplifying the detection process. Furthermore, since the 1's and 0's in the scrambling sequence are interleaved across the bit duration, the above process results in comparing the changes in the signal over a much shorter 'chip duration'. As the changes in the channel over chip duration are

significantly less, compared to those of a much longer 'bit duration', this detection scheme has an increased tolerance to channel fading. A simple implementation of this comparison process is shown in Figure 3.4, by mapping the 1's and 0's of scrambling sequence with 1, and -1, respectively, and multiplying it with the sequence $R(k)$. The Rx can now generate a decision variable Y from the above comparison, as shown in the figure.

However, before implementing the detection logic to decode the transmitted data bit, the Rx also has to adjust for the relative phase differences in the channels. Since the phase changes in the different links are independent to each other, the reflected backscatter signal may both add, or subtract the energy of the total received signal, depending on the relative phase difference across the channels. Therefore, the Rx requires a crude estimation of the channel to adjust its decision logic, based on these relative phase changes. A detailed mathematical derivation, not shown in this report, concurs that the Rx has to flip its decision logic when the channel coefficients satisfy the condition

$$\left|1 + \frac{h_f h_b}{h_i}\right|^2 - 1 < 0. \tag{3.9}$$

The implementation of this channel correction is shown in Figure 3.4, where the Rx adjusts its detection, based on the 'sign' of the above equation. Finally, the Rx can now detect the transmitted bit d, using 0 as its decision threshold as follows

$$Y \underset{d=0}{\overset{d=1}{\gtrless}} 0. \tag{3.10}$$

Note that the above description is a simplified explanation using key points. Interested readers can perform a detailed derivation for the ML detection using the same channel assumptions, and find that the derivation also leads to the above steps, showing that the Rx structure in Figure 3.4 is in fact, an ML detector under the previously assumed Quasi-static nature of the channels.

So far, we have described the detection at the Rx, under the Quasi-static channel assumption. However, the above detection scheme fails for the case where the channel is not constant within the bit duration. In this case, the Rx needs to implement the channel correction for the fading occurring within the bit duration. For this, an alternative Rx structure is presented in Figure 3.5, where the channel correction based on (3.9) is implemented before the Rx sums up all the chip energies, and generates the decision variable. Here, it is worth mentioning that this alternative Rx structure no longer follows ML detection, as the channel corrections are performed using the 'sign' of (3.9) for simplicity, and not the actual coefficients that are needed for an ML detector. But on the other hand, this alternative Rx structure is capable of correcting the changes in the channel for each chip duration, which can significantly reduce the effects of continuous fading. However, implementing such algorithm requires more frequent channel estimations at the Rx, which increases its complexity and power consumption. But we nonetheless investigate the limits on when such a Rx works sufficiently well, in the upcoming chapter.

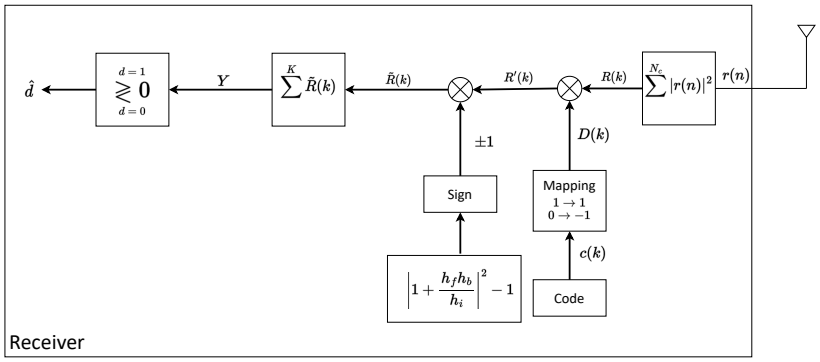

Figure 3.5: Block diagram for alternative Rx with channel correction for each chip duration.

3.5 Link Budget

In this section, we set up the AmBCS link budget, and derive the analytical expression for the Signal to Interference plus Noise Ratio (SINR) at the Rx. We also calculate a simple expression for the Signal to Interference Ratio (SIR) at the Rx. These expressions are used to analyze the performance of AmBCSs in the next chapter. Figure 3.6 illustrates the overall link budget of a typical AmBCS. As shown in this figure, the link budget for an AmBCS can be divided into the forward link, backscatter link, and the interference link components. This figure also shows the SIR for the AmBCS, which is a difference between the received power levels of the interference and the backscatter signal components.

Let us now follow each of the links and formulate the expressions for each individual received signal power levels. Following Figure 3.6 for the forward link, the received signal power at the backscatter device can be expressed as

$$P_{in} = P_T + G_T - L_f - X_f + G_B, \tag{3.11}$$

where P_T is the ambient RF source transmit power, G_T and G_B are the antenna gains of RF source and backscatter device, respectively, X_f the forward link polarization mismatch, and L_f the path loss in the forward link.

Similarly, following the backscatter link in Figure 3.6, the received backscatter signal power at the Rx can be expressed as

$$P_{bsc} = P_{out} + G_B - L_b - X_b + G_R, \tag{3.12}$$

where G_R is the antenna gain of the Rx, X_b the polarization mismatch in backscatter link, L_b the path loss in the backscatter link, and P_{out} the reflected signal power at the backscatter device, which can be written as

$$P_{out} = P_{in} - \Gamma, \tag{3.13}$$

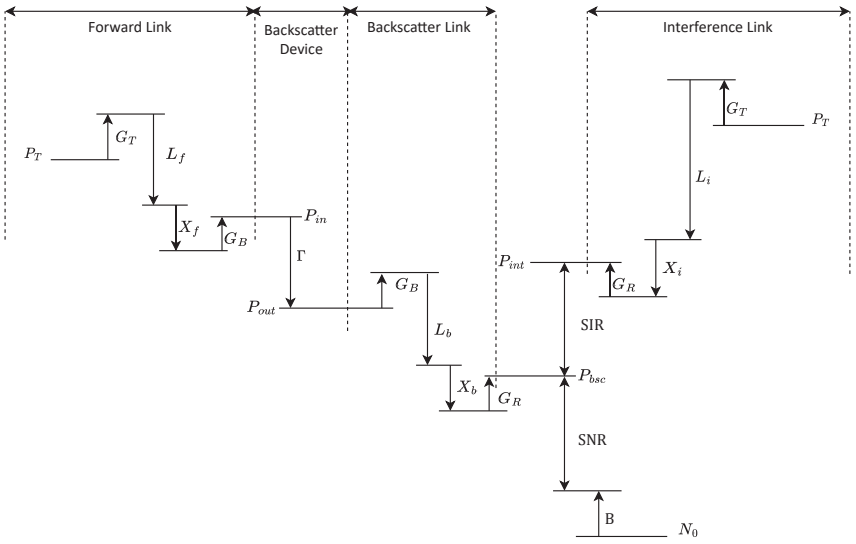

Figure 3.6: A simple link budget illustrating the SIR for AmBCSs.

where Γ is the reflection efficiency at the backscatter device in dB. Earlier in Section 2.1, we have described the ideal values for reflection coefficient as, $|\gamma| = 0$ for perfect absorption, and $|\gamma| = 1$ for perfect reflection. However, it may not be possible to realize these ideal values for $|\gamma|$ at the backscatter device, and the practical values can be slightly deviated, resulting in reduced reflection efficiency at the backscatter device, denoted as Γ in the Figure 3.6, where $\Gamma = |\gamma|^2$. Although the reflection efficiency (Γ) contributes to small changes in the signal power, compared to the path losses, we nonetheless include it to set up our link budget to the greatest detail possible. Considering above and substituting (3.11) and (3.13) in (3.12), the received backscatter signal power at the Rx becomes

$$P_{bsc} = P_T + G_T + 2G_B + G_R - L_f - L_b - X_f - X_b - \Gamma. \tag{3.14}$$

As described earlier, the ambient RF signal is also received as direct interference at the Rx. The signal power for this interference at the Rx, following the interference link in Figure 3.6, can be expressed as

$$P_{int} = P_T + G_T - L_i - X_i + G_R, \tag{3.15}$$

where X_i, and L_i are the polarization mismatch and path loss in the interference link, respectively.

Now that we have the link budget expressions for all individual received signal power levels, let us proceed to formulate the expressions for SINR, and SIR. The SINR at the Rx, however, cannot be seen directly in the link budget figure, but expressed in linear scale as

$$\text{SINR} = \frac{P_{bsc}}{P_{int} + P_n}. \tag{3.16}$$

where P_n is the noise power at the Rx, and P_n is typically given as

$$P_n = N_0 B, \tag{3.17}$$

where N_0 is the noise spectral density and B is the bandwidth of the received RF signal.

To derive a complete linear expression for the SINR, the path losses in the forward link, backscatter link, and the interference link need to be calculated in linear scale, using a suitable propagation loss model. Denoting the distances between the components in the forward link, backscatter link, and interference link shown in Figure 3.1 as d_f, d_b, and d_i, respectively, we calculate the path loss using a variation of the free-space propagation formula, expressed in decibel (dB) as

$$L_x = 10 \log_{10} \left(\frac{\lambda}{4\pi d_x} \right)^{\eta}, \quad x \in (f, b, i), \tag{3.18}$$

where λ is the RF wavelength, and d_x the propagation distance, η the path-loss exponent. Note that, in this link budget calculation, we formulate the path-losses using the free-space propagation loss model, where, $\eta = 2$. However, we will use this same propagation loss model later, while evaluating the AmBCS performance for different propagation environments, by allowing η to take on values other than 2.

Now, by converting (3.14), (3.15) and (3.17) to linear scale and substituting in (3.16), we get the complete expression for SINR as

$$\text{SINR} = \frac{\frac{\Gamma P_T G_T G_B^2 G_R}{X_f X_b} \left(\frac{\lambda^2}{(4\pi)^2 d_f d_b} \right)^{\eta}}{\frac{P_T G_T G_R}{X_i} \left(\frac{\lambda}{4\pi d_i} \right)^{\eta} + N_0 B}. \tag{3.19}$$

As we can see, due to the presence of the Rx noise $N_0 B$ in the denominator, the expression for SINR in (3.19) is complicated and therefore, relatively more difficult to analyze. However, if we can factor out the Rx noise from the above expression, we get a much simpler expression for the SIR as

$$\text{SIR} = \frac{\Gamma G_B^2}{X_f X_b X_i} \left(\frac{\lambda}{4\pi} \frac{d_i}{d_f d_b} \right)^{\eta}. \tag{3.20}$$

Given the simplicity of SIR in (3.20) compared to that of SINR in (3.19), we can see that, the variables can be modified easily using (3.20) for analyzing the AmBCS performance across different scenarios. Keeping this in mind, we examine whether it is reasonable to factor out the Rx noise in AmBCSs through simulations in the next chapter. We also present the simulation results and evaluate the performance of the AmBCS across different channel, and propagation conditions, and analyze the relations among different performance metrics.

Chapter 4

Results and Performance Evaluation

In this chapter, we present the simulation results, and discuss the AmBCS performance across different scenarios. We describe the simulation parameters, channel models and propagation environments used in the simulations in Section 4.1 and discuss the reasons behind these assumptions. We also describe our coverage illustration model, which is a geographical depiction of AmBCS coverage that can be easily understood, and compared across various scenarios. As we previously discussed, factoring out the Rx noise makes it easier to simulate and allows us compare the AmBCS performance across various scenarios using SIR. Therefore, in Section 4.3, we will study the conditions where AmBCSs are more or less, completely defined by the interference level, and the Rx noise can be safely ignored. In Section 4.3, we discuss the AmBCS performance using simple channel models. BER, data-rate, and coverage are all important parameters in defining the performance of a communication system. It is therefore, interesting to study the relations among these parameters. Hence, we also analyze the relations among the BER, data-rate, and coverage of AmBCSs across different propagation environments and RF frequencies. Although Section 4.3 provides us with a good overview of AmBCS performance across different scenarios, the channel models used in this section may not be realistic for all cases. Therefore, in Section 4.4, we will discuss the AmBCS performance under continuous fading conditions, using a more realistic Extended Pedestrian A (EPA) channel model. Let us start by describing the simulation setup, and an explanation for visualizing the AmBCS coverage, that are used for the performance analysis in this chapter.

4.1 Simulation Setup and Visualization

The simulations for evaluating the AmBCS performance, are performed using Monte-Carlo simulations in MATLAB. The baseband ambient RF signals used in the simulations are modeled as band limited complex Gaussian noise as described in Section 3.1. The antennas for all components in our system model are assumed as isotropic, and their antenna gains G_T, G_B, and G_R, are set to 0 dBi. The backscatter device is assumed to have perfect reflection efficiency (i.e., $|\Gamma| = 0$), and the polarization mismatch for different links, X_f, X_b, and X_i, are also assumed to be 0 dB. The sampling frequency for the ambient RF signal can be set to any desired value. However, we use a sampling frequency of $f_{samp} = 30.72$ MHz [29],

to put our analysis in the 3GPP context. The carrier frequencies for the ambient RF signal are chosen as 900 MHz, 1800 MHz, and 2.4 GHz, as they are widely used in many typical ambient RF sources. The repetition factor (N) is treated as a variable in our simulations, with its values ranging from 100 to a million samples per bit. The above range of N used in the simulations also corresponds to a wide range of backscatter data-rates where the data-rate (R_b) for any particular repetition factor N, is calculated using $R_b = f_{samp}/N$. The wide range of potential use-cases for AmBCSs means that the AmBCS performance should be studied across different propagation environments, and channel models. Let us first discuss different channel models used in the simulations in the following subsection.

Channel Models

The simulations discussed in this chapter are performed using two different channel models: a simple model with quasi-static fading, where the channel is assumed to be constant over a bit duration, and a realistic model, where the channel is assumed to be fading continuously and also within the bit duration. Here, we describe these two channel models in more detail, and the reasons behind these channel assumptions.

The devices in most of the backscatter applications discussed in Chapter 1 are typically expected to be stationary, implying that the channels in AmBCSs do not change very rapidly in time. Therefore, we can reasonably assume a simple channel model with quasi-static properties, i.e., the channel in each link stays constant over the bit duration. In this quasi-static channel model, we generate the complex channel gains of individual links (h_f, h_b, and h_i) for each bit duration according to a two-dimensional circularly symmetric Gaussian distribution, with consequent Rayleigh distributed amplitudes. Furthermore, the fading characteristics of this Quasi-static channel model are modified to obtain Rician fading with different K - factors, by adding an appropriate fraction of Line Of Sight (LOS) component, to the channel gains of Rayleigh fading. As mentioned earlier in this chapter, we use these quasi-static channels to perform simplified analysis across different scenarios later in Section 4.3.

However, the conclusions drawn from the quasi-static channel models may not be realistic due to their simplicity. Therefore, we also use a second channel model with continuous fading, where we study the limits for which the results for the quasi-static channel are no longer valid due to fading. For this purpose, we choose the standard EPA channel model specified by 3GPP, with a Doppler spread of 5 Hz. The parameters of the EPA model are presented in Table. 4.1 [30]. The multi path delay profile of the selected Doppler spread of this channel model represents a low delay spread environment, making it suitable for backscatter applications in slow moving environments. The results for this continuous fading channel are discussed in Section 4.4. Now, having the channel models described in detail, let us move on to the next subsection and discuss different propagation environments.

Excess tap Delay (ns)	**Relative power** (dB)
0	0.0
30	−1.0
70	−2.0
90	−3.0
110	−8.0
190	−17.2
410	−20.8

Table 4.1: Parameters of 3GPP EPA-5 channel model.

Propagation Environments

When performing analysis, we assume different propagation environments, with their corresponding path loss exponents to estimate the AmBCS performance over a wider range of environments.

We know that the standard and simple approach to calculate path loss is using Friis' free-space propagation, i.e., assuming the path loss exponent as $\eta = 2$. However, this assumption is not universal, and the results in the real world often differ depending on the nature of the measured environment. For instance, in the case of an indoor environment, the propagation distances are very small, and the confined spaces provide a rich multi path environment. Therefore, the propagation loss in indoor environment is typically low, and the path loss exponent can be expected to be as low as $\eta = 1$. Similarly, in case of outdoor environment, the multi-path components may not exist due to the long distances involved. Therefore, the path loss exponent for outdoor environments is normally specified as $\eta = 4$, assuming that only LOS and a ground-reflected wave exist. Furthermore, different links in an AmBCS can also experience different path loss exponents, depending on the type of use-case scenarios. Let us consider an AmBCS, where the backscatter link experiences a better propagation environment compared to the other two links, as shown in Figure 4.1. Such a scenario is possible, for instance, when the Rx and backscatter device are located in a free-space environment, while the ambient RF source is located far away in an outdoor location. In this case, the path loss exponent for the backscatter link is $\eta = 2$, while it is $\eta = 4$ for both forward link and interference link. It is also interesting to analyze the AmBCS performance in such asymmetrical propagation environments. Therefore, we consider the case in Figure 4.1 as a special case, and use it for comparison with the typical outdoor environment. Lastly, it is also important to choose reasonable distances between the Rx and the ambient RF source for each propagation environment.

The different propagation environments used in our analysis and their corresponding path loss exponents and interference link distances are listed as follows:

- Indoor environment ($\eta = 1$, $d_i = 10$m)
- Free-space environment ($\eta = 2$, $d_i = 2$m & 10m)

- Outdoor environment ($\eta = 4$, $d_i = 100$m)
- Asymmetric environment ($\eta = 4$ & 2, $d_i = 100$m)

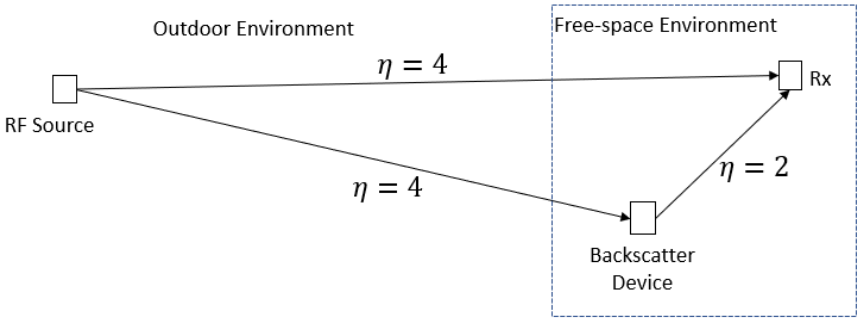

Figure 4.1: A possible scenario for an asymmetrical propagation environment in an AmBCS.

Coverage Area Illustration

The placement of system components and the distances between them in AmBCSs can greatly vary depending on the applications, and the environments that they are deployed in. For example, the distance between the ambient RF source and the Rx in outdoor environments can be typically many times longer than that of indoor environments. Moreover, the absolute distances between the devices also depends on the specific requirements of AmBCS designs, and their use-cases. Therefore, it is important to understand the coverage characteristics of AmBCSs over a variety of environments. For this purpose, we discuss the AmBCS coverage using a simple illustration that depicts the coverage area surrounding the ambient RF source and the Rx, within which the backscatter device can reach certain BERs, and data-rates.

Let us now describe the illustration of coverage visualization in more detail. Figure 4.2, with its distance axes, shows the contour maps for the coverage around the Rx and the ambient RF source, for different levels of SIR. Each contour line in this figure represents the boundary area for a particular SIR level, meaning that the backscatter device can achieve a particular SIR, when deployed within its corresponding contour line. Since it is more likely that the backscatter devices are placed near the Rx, rather than the ambient source, we set the coordinates for the Rx as the origin, and place the ambient RF source on the x-axis, at a distance of d_i. This makes it easier to comprehend the coverage distances without complex calculations. With the right knowledge of the relation between SIR and the repetition factor, one can easily translate the SIR levels in Figure 4.2 to the AmBCS data-rates, to find the coverage for any particular data-rate. We use this simple model for studying the AmBCS coverage in the upcoming sections, using

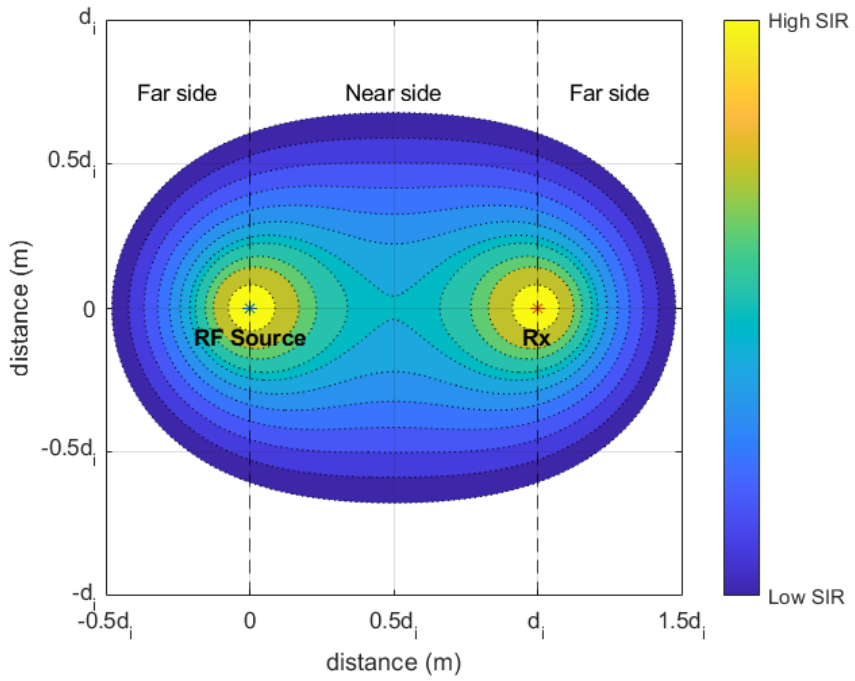

Figure 4.2: A geographical illustration showing contour maps for AmBCS coverage at different SIR levels

different values of d_i, and plot the coverage contours for different combinations of data-rates, BER requirements, RF frequencies, and propagation environments.

Now that we have described all the necessary details of simulation setup and coverage visualization, let us move on to analyzing the AmBCS performance. Let us start by studying the influence of Rx noise on the AmBCS performance in the following section.

4.2 Influence of Rx noise

Earlier in Section 3.5, we have seen that the expression derived for the SINR is complicated, and relatively difficult to analyze. We have also discussed that, by factoring out the Rx noise, we can simplify the expression of SINR to SIR, and easily manipulate the variables for analyzing the AmBCS performance across multiple scenarios. However, it is also important to study the conditions when the Rx noise can be safely ignored. In this section, we simulate the AmBCS model using different levels of Interference to Noise Ratio (INR) and study the influence of Rx noise. We use a noise-free AmBCS model as reference for comparison. Through this simulation, we aim to identify a threshold for INR where the Rx noise is negligible compared to the interference and has little to no effect on AmBCS performance.

Figure 4.3 shows the BER contour curves as a function of repetition factor (N), and the required SIR (in dB) at 10% BER, and for different INR levels (in dB). This simulation is performed using a quasi-static Rician channel model, and assuming pure LOS (i.e., K-factor $= \infty$). It can be observed from Figure 4.3 that,

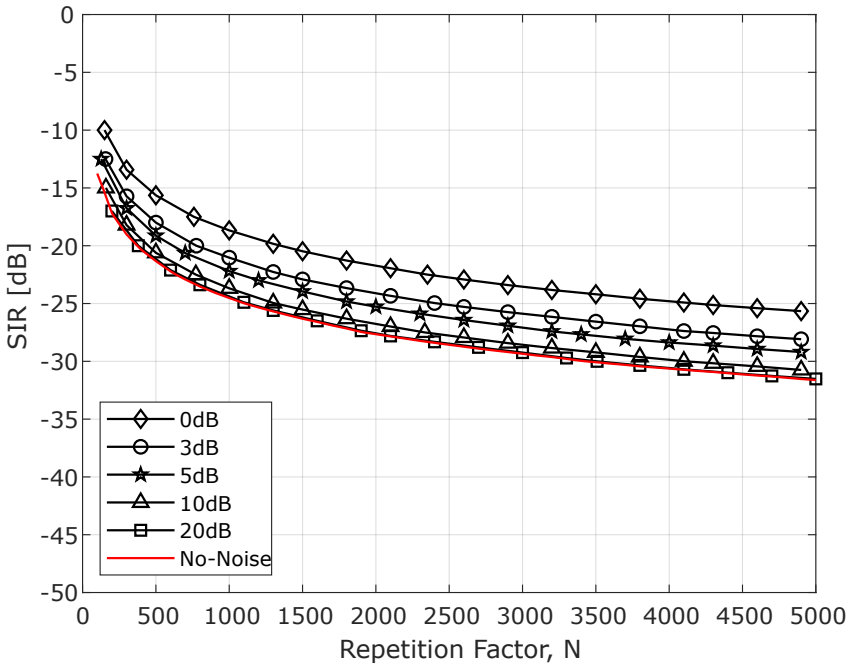

Figure 4.3: Contour curves as a function of SIR and spreading factor,N at 10% BER requirement, for different INR levels. Contour curve with no-noise contribution is shown (in red) for reference.

when the Rx noise level increases, a higher SIR level required to reach the 10% BER, at a given repetition factor. However, we can see that the contour curves for the cases of INR $\geq$ 10 dB are approximately equivalent to that of no-noise at the Rx, and any notable deviation in the contour curves compared to the no-noise case can be observed only for INRs below 10 dB. Therefore, these results suggest that the Rx noise can be safely ignored for the cases where INR $\geq$ 10 dB is fulfilled. It is also worth mentioning that the results for the above simulation, performed at 1% BER requirement also exhibit similar trend, leading to the same conclusions.

Here, let us recall that the backscatter signal experiences the path-loss twice before reaching the Rx, while the interference signal undergoes path-loss only once. This means that the interference is typically much stronger, compared to the backscatter signal. Meanwhile, a weak interference signal means that the backscatter signal is much weaker, and is possibly undetectable. Therefore, it is reasonable to assume that the interference has some substantial power in practical

cases, and is also significantly stronger than the Rx noise. Therefore, we can safely consider that the condition of INR $\geq$ 10 dB in AmBCSs will be most likely fulfilled, and we can factor out the Rx noise from the simulations discussed in the upcoming sections. Let us also note that the Rx noise is typically generated within the Rx and is not affected by the choice of the channel model. Therefore, the above conclusions are not just restricted to the 'Pure LOS' channel, they can also be applied to other channel models that are used in the later sections.

The above condition INR $\geq$ 10 dB sets a boundary for the maximum separation d_i between ambient source and the Rx within which the Rx noise can be neglected. This boundary for d_i can be calculated by rearranging the expression for P_{int} in (3.15) and applying the condition $P_{int}/P_n \geq 100$ as,

$$d_i \leq \frac{\lambda}{4\pi} \left[\frac{{\sigma_s}^2}{10{\sigma_w}^2} \right]^{\frac{1}{\eta}}. \tag{4.1}$$

Here, we consider that the Rx noise is sufficiently low, and assume that the above condition is met for the discussions in the following sections. However, with the knowledge of the ambient RF signal transmit power, and the Rx noise level, one can verify the condition in (4.1) for practical cases, and know the range of d_i for which, the above-mentioned simplification for the Rx noise is valid. Now, we know the impact of Rx noise on AmBCSs, and have defined a safe threshold for factoring it out from our analysis. Let us now discuss the AmBCS performance in more detail in the following section, using the quasi-static channel models.

4.3 Performance Analysis across Quasi-static Channels

In this section, we study the relation between the SIR and the repetition factor, for understanding the effectiveness of repetition technique in addressing the strong interference at the Rx. We study this for two different BERs, using quasi-static channels with different fading characteristics, described in Section 4.1. We also evaluate the relations among the BER, data-rate and coverage metrics of AmBCSs across different RF frequencies, and propagation environments, also described in Section 4.1.

In Figure 4.4, we show the BER contour curves as a function of repetition factor N, and SIR (in dB), at 10%, and 1% BERs, across the quasi-static channel models with Rayleigh, and Rician (with different $K-$factors) fading characteristics. Let us first analyze the relation between the required SIR level and the repetition factor, N. When the backscatter bit is repeated over N samples of the ambient RF signal, the backscatter signal strength at the Rx is increased by a factor of N. Consequently, the processing gain at the Rx is also increased N times, thus improving the tolerance to interference. Therefore, one can expect a decrease in the required SIR level, when the repetition factor is increased. Comparing the BER contours in the Figure 4.4, across all channel models in both BER cases, we observe that the required SIR level drops when N is increased, with an 'inversely proportional' relation, which supports the above expectation. These results show that, the required SIR level can be decreased to a desired value, by sufficiently increasing N.

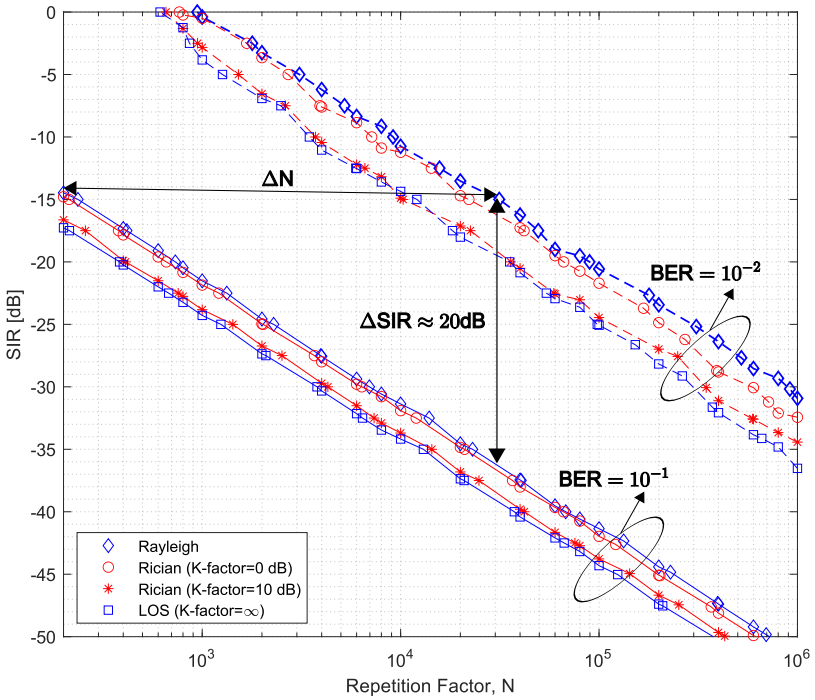

Figure 4.4: BER contour curves as a function of required SIR and Repetition factor N, across quasi-static channel models at 10%, and 1% BERs.

Let us now look into the BER contours in the Figure 4.4, for each individual quasi static channel distribution, and study the influence of LOS component in AmBCS performance. Here, we consider the quasi-static Rayleigh channel case as our reference for comparison. We observe that the difference in the required SIR between, the pure LOS model, and the Rayleigh model, for any given value of N, is limited to 3-5 dB. In fact, the results for the Rician model, with a reasonable $K-$ factor of 0 dB, are almost equivalent to the Rayleigh channel case. This shows that the LOS component has little significance in altering the AmBCS performance.

Furthermore, it is also interesting to observe the difference in the simulation results in Figure 4.4 across different BER levels. We learn from the results that, at any particular SIR level, the repetition factor should be increased by a factor of ΔN, for the AmBCSs to achieve a better BER of an order 1 (i.e., 10 times lower BER). Since $R_b \propto 1/N$, and a constant SIR requirement means an unchanged coverage, these results means that the R_b of AmBCSs must be reduced ΔN times, in order to reach a better BER of an order 1, without loosing any coverage. Similarly, at any given repetition factor, the required SIR level increases by ΔSIR,

when the AmBCSs reach a better BER of an order 1. Since an increase in the required SIR level means a shorter coverage, we can interpret that better BERs can be achieved by moving the backscatter device closer to either the Rx or the ambient RF source. These observations reflect that there exists relations among the BER, data-rate, and the coverage metrics of AmBCSs.

To have a better understanding of these relations, we study the AmBCS coverage for different data-rates and BERs, across different RF frequencies, and propagation environments in the following discussions. For this purpose, we use the coverage illustration, described earlier in Section 4.1 and discuss the AmBCS coverage for two scenarios which demonstrate:

- the relation between different data-rates, and BERs, that result in similar coverage, and
- more detailed characteristics of AmBCS coverage across different propagation environments.

Let us first look into the combinations of different data-rates and BERs, that provide similar coverages. Figure 4.5 shows the coverage contour maps as a function of distances (in m), across different RF frequencies and propagation environments, and for different combinations of BERs and data-rates. The coverage contours in this figure are generated using the simulation results of the quasi-static Rayleigh channel shown in Figure 4.4. As previously mentioned, the Rx is placed at the origin, and the ambient RF source is placed at a distance d_i from the Rx along the x-axis. The values taken for d_i in each propagation environment, are also shown in the figure.

Comparing the subplots in Figure 4.5 across frequency, we see that the coverage drops when the ambient RF frequency increases, which is expected. Similarly, we see that the coverage also drops when the path-loss exponent increases, which is also expected, due to greater path losses. However, we can observe across all subplots that, the coverages for specific combinations of BERs, and data-rates, are similar. Here, we see that the data-rate at 1% BER is 100 times slower than the data-rate with same coverage at 10% BER. For example, the coverage for 100 kbps at 10% BER is the same as that for 1 kbps at 1% BER. This means that the AmBCSs can either

- transmit at 100 times faster data-rate, and with a BER of 10%, or
- transmit at 100 times slower data-rate, and with a BER of 1%,

while maintaining the same coverage. Here, we can comment that it is more reasonable for AmBCSs to settle for low data-rates, and more reliable BERs, to meet the massive IoT needs of reliably transmitting small amounts of data. Having discussed the relation between data-rate, BER, and coverage, let us now look into the coverage characteristics of AmBCS, for each propagation environment in more detail. The coverage characteristics in all the following descriptions are studied for three RF frequencies, i.e., 900 MHz, 1800 MHz, and 2.4 GHz, and two different BERs, i.e., 10%, and 1%. Let us start with an indoor environment below.

Figure 4.6 shows the AmBCS coverage contour maps in an indoor propagation environment and at an interference link distance of $d_i = 10$m, for different

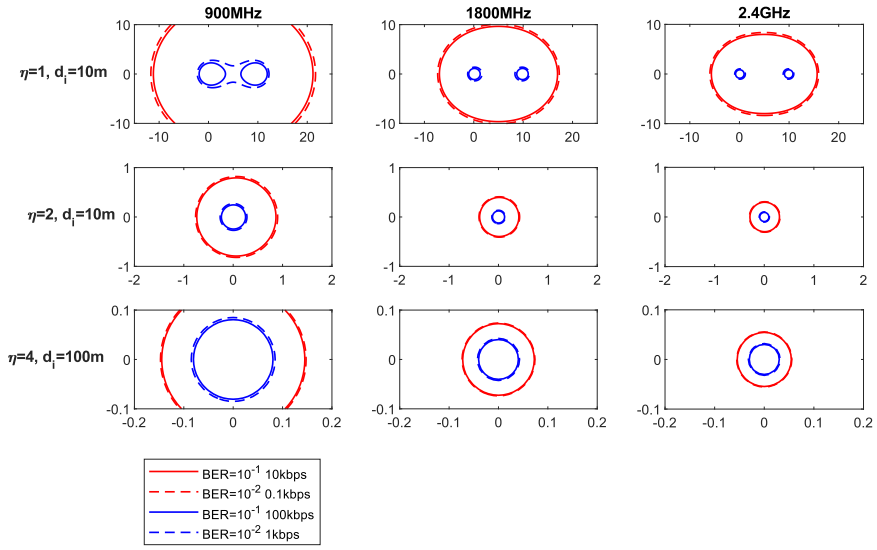

Figure 4.5: AmBCS coverage contour maps for different BER, and data-rate combinations, with similar coverage. Distances on x, and y axes in meters.

data-rates. As we discussed earlier, the backscatter signal energy at the Rx can be increased by transmitting the bits at a lower data-rate, and this means that greater coverage can be expected for lower backscatter data-rates. This is visible across all subplots in Figure 4.6, where the coverage for low data-rates are significantly larger than that for high data-rates. Here, let us consider the coverage results for the data-rates 0.1 kbps and 1 kbps, at a carrier frequency of 1800 MHz, and compare them across each propagation environment to understand the coverage characteristics. The conclusions from these comparisons can also be more or less applicable across other data-rates and carrier frequencies, with a few minor differences. In the indoor propagation environment, the data-rates 0.1 kbps and 1 kbps at a BER of 10%, have an approximate coverage of 120m and 40m, respectively. Meanwhile, the coverage for the same two data-rates at a BER of 1%, has a coverage of 15m and 2m, respectively. These results show that, for a 1 order improvement in the BER, the coverage in the indoor environment drops by a factor of around 8-20 times, depending on the data-rate. Furthermore, we can observe that the coverage for any higher data-rate at 1% BER is confined to the area close to the ambient RF source and the Rx, too small for practical applications. Let us now look into the free-space propagation environment, and discuss the coverage characteristics using different interference link distances.

Figure 4.7 shows the AmBCS coverage contour maps in a free-space propagation environment, across different RF frequencies, at 10% and 1% BERs, and

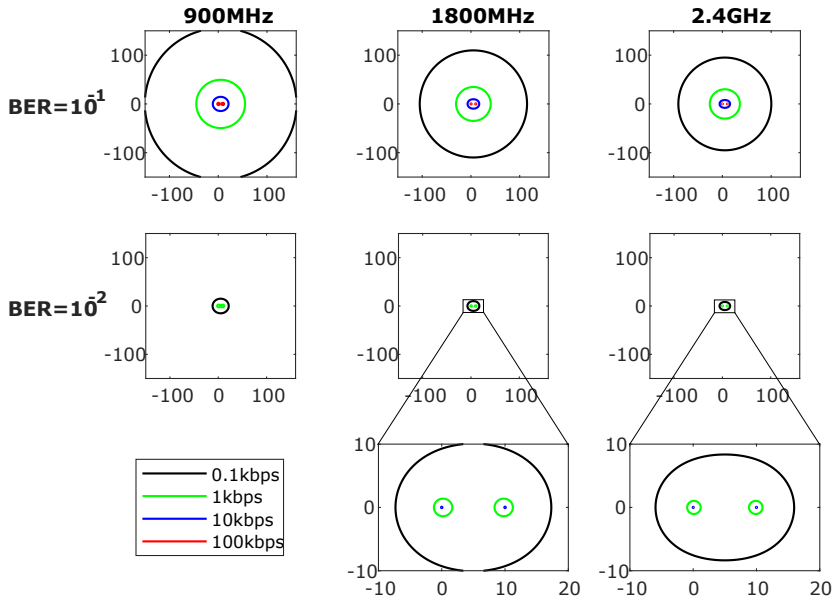

Figure 4.6: AmBCS coverage contour maps for an indoor propagation environment ($\eta = 1$) for $d_i = 10$m. Distances on x, and y axes in meters.

for different data-rates. The coverage contour maps in Figures 4.7a and 4.7b are shown for interference link distances of $d_i = 2$m and $d_i = 10$m, respectively. The results in the Figure 4.7a shows that the coverage for the data-rates 0.1 kbps, and 1 kbps at a BER of 10%, are approximately 4m and 2.5m, respectively. Similarly, the coverage for the same two data-rates at a BER of 1%, are approximately 0.5m and 0.1m, respectively. However, in Figure 4.7b, we see that the coverage for 0.1 kbps at 10% BER is around 12m, whereas that for 1 kbps is around 1m. This is an interesting result, as the increase in d_i from 2m to 10m at 10% BER resulted in around 3 times increase in coverage for the lower data-rate (0.1 kbps) whereas, the coverage for the higher data-rate (1 kbps) is in fact, reduced. However, for the case of 1% BER, the coverage contours in Figures 4.7a and 4.7b remain almost the same, and the change in coverage due to the increase in d_i is minimal. This shows that the distance between the Rx and the ambient RF source (d_i) also has an influence, and can affect the AmBCS coverage differently for different data-rates and BERs. Furthermore, comparing the free-space environment results in Figures 4.7a and 4.7b with the indoor environment in the Figure 4.6, we can see that the coverage distances in free-space are around $20 - 40$ times shorter than that of the indoor environment. Let us now move on, and discuss the coverage characteristics in an outdoor environment, along with a special case of an asymmetric outdoor environment.

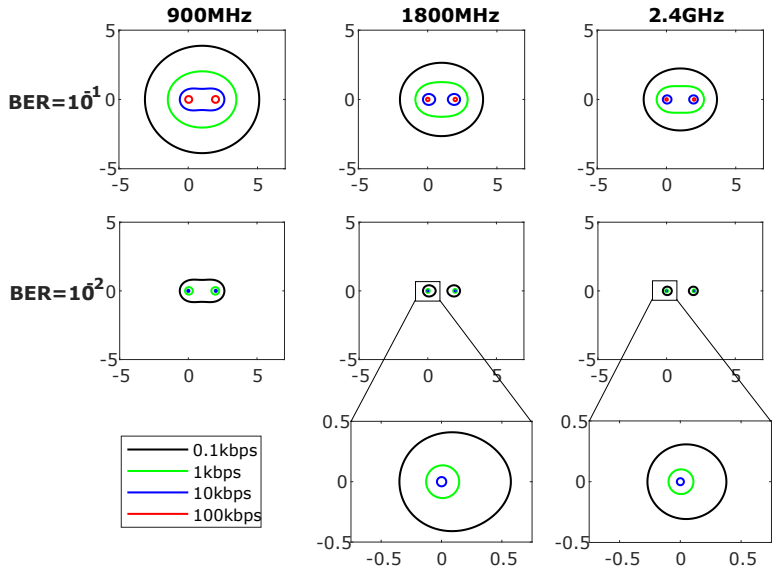

(a) $d_i = 2$m

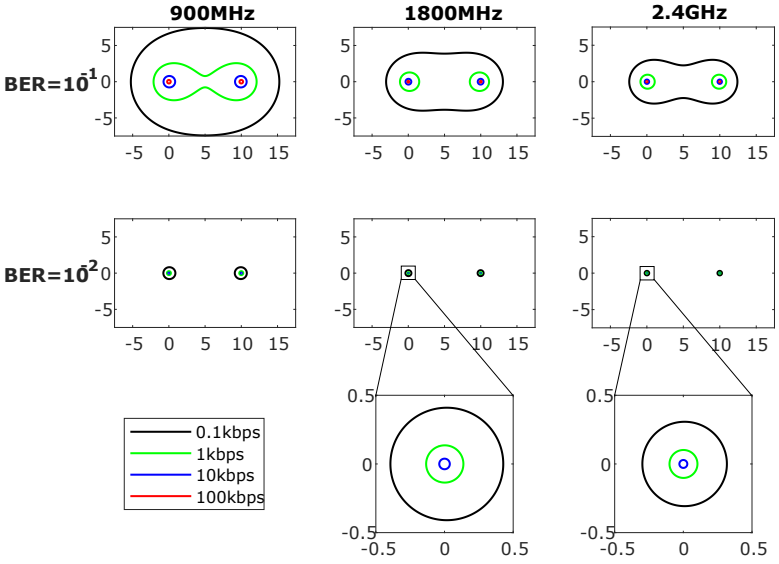

(b) $d_i = 10$m

Figure 4.7: AmBCS coverage contour maps for a free-space propagation environment ($\eta = 2$) for different d_i(in meters). Distances on x, and y axes in meters.

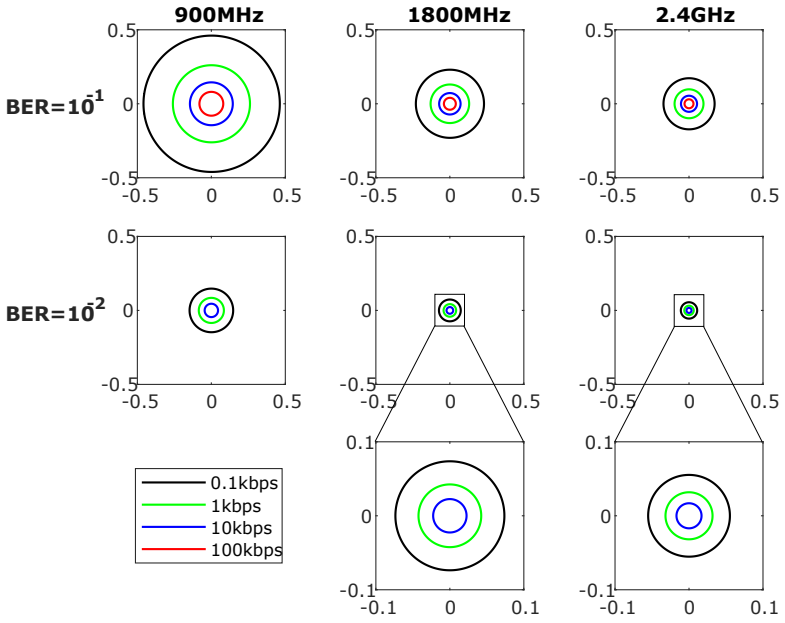

(a) Typical outdoor environment ($\eta = 4$)

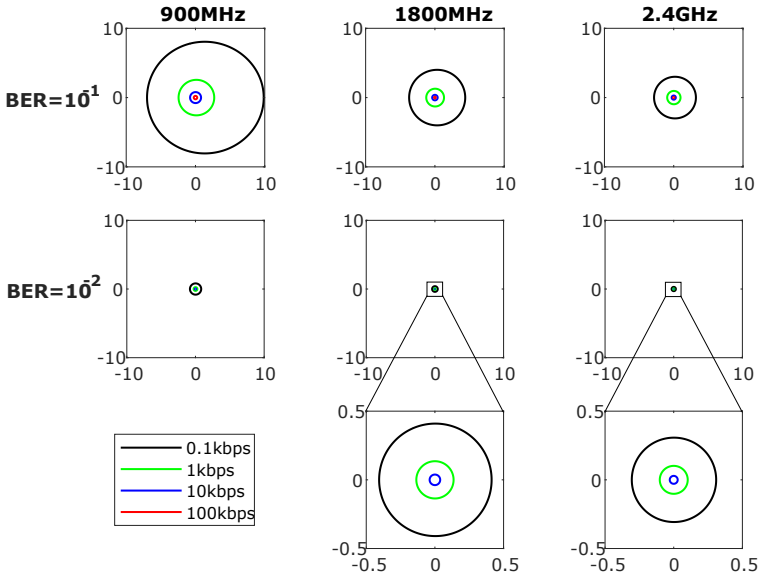

(b) Outdoor environment with better propagation in the backscatter link ($\eta = 4$ & 2)

Figure 4.8: AmBCS coverage contour maps for outdoor environments with $d_i = 100$m. Distances on x, and y axes in meters.

Figure 4.8 shows the AmBCS coverage contour maps in an outdoor propagation environment with d_i = 100m, across different RF frequencies, at 10% and 1% BERs, and for different data-rates. The coverage contour maps in Figure 4.8a are shown for a typical outdoor environment with a path loss exponent of $\eta = 4$ across all three links of an AmBCS. On the other hand, Figure 4.8b shows the coverage contour maps for the AmBCS setup described earlier in the Figure 4.1, where the path loss exponent is $\eta = 2$ for the backscatter link, and $\eta = 4$ for both the forward link and the interference link.

It can be seen in Figure 4.8a, that the actual coverage distances in the outdoor environment are much shorter, compared to the indoor and free-space environments. As can be seen in Figure 4.8, the coverage distance for data-rates 0.1 kbps and 1 kbps at 10% BER, are confined to around 0.25m and 0.1m, respectively. Similarly, the coverage for the same two data-rates at a BER of 1%, are confined to 0.08m and 0.05m, respectively. These distances are extremely short, compared to the results in the previous propagation environments, and are hardly useful for practical applications. However, it is to be noted that these coverage distances are derived assuming no antenna gain at the Rx. Therefore, for the cases where the high-gain/multiple antennas are used at the Rx, the SIR levels can be improved, and longer coverage distances can be expected than the results in Figure 4.8a. In addtion, better results in coverage can be expected if we consider the special case where, at least one of the links in the backscatter signal path, can experience a better propagation environment. Let us study the coverage results of Figure 4.1, to look into this aspect.

The results in the Figure 4.8b show that the coverage for the data-rates 0.1 kbps and 1 kbps at a BER of 10%, are approximately 10m and 2m, respectively. Similarly, the coverage for the same two data-rates at a BER of 1%, are approximately 0.4m and 0.1m, respectively. Comparing these results with that of Figure 4.8a, we find that, substantial improvements in AmBCS coverage can be achieved, by optimally adapting the backscatter link environment, even if the other two links face significant path losses, and if the ambient RF source is located at much greater distance from the Rx and the backscatter device.

4.4 Performance Analysis across EPA channel

As described earlier, the channel models used for simulations in the previous section assume quasi-static fading. Quasi-static assumption means that the channel is always constant over the bit duration (T_b), and the condition $T_{coh} \gg T_b$ is always met, even when T_b is increased indefinitely. But this assumption is not realistic as in reality channels fade continuously and their T_{coh} are typically very small. Therefore, in this section, we study the influence of fading occurring within T_b on the AmBCS performance and also discuss the breaking-points of both repetition and scrambling techniques, under continuous fading. Here, we also evaluate the effectiveness of implementing scrambling for making the Rx less susceptible to fading.

Figure 4.9 shows the BER contour curves as a function of repetition factor N, and SIR (in dB), at 10%, and 1% BERs, across the EPA channel model for the

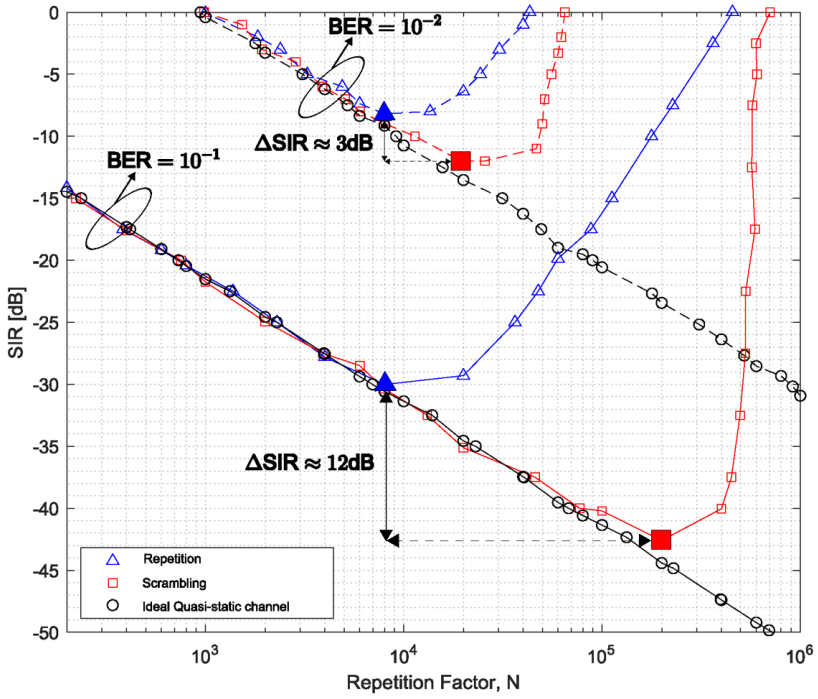

Figure 4.9: BER contour curves for SIR vs Spreading factor across EPA channel at 10%, and 1% BERs comparing repetition, and scrambling techniques.

repetition, and scrambling techniques. The parameters of the EPA channel model used in these simulations are described earlier in Section 4.1. The BER contour curves for a quasi-static Rayleigh channel model are also shown in Figure 4.9 for comparison. From the BER contour curves of quasi-static channel, we observe that the required SIR level keeps descending indefinitely, when the repetition factor increases. In case of the EPA channel, it can be seen that both repetition and scrambling techniques follow the same behavior as in quasi-static channel at low repetition factors. This is because the bit duration is small enough at low repetition factors, so that the condition $T_{coh} \gg T_b$ is met, and the EPA behaves similar to the quasi-static channel. However, while increasing the repetition factor to greater values, we can see from Figure 4.9 that the relation between the required SIR level and the repetition factor, N, reverses for both repetition and scrambling techniques, at different points. Let us now discuss the reasons behind this behavior for both techniques, one by one.

As mentioned earlier, the Rx makes a decision for the repetition technique by aggregating signal energy over the entire bit duration. We also know that higher repetition factor means longer bit duration. Therefore, by comparing the signal energies over such long duration, where the channel could have changed significantly,

the Rx makes wrongful decisions at high repetition factors. This explains the trend observed for the BER contour curves for repetition in Figure 4.9. However, in the case of scrambling, each bit is divided into multiple chips, each with duration T_c, where $T_c \ll T_b$. Therefore, the Rx can now compare the received signal energies over each chip duration, which are relatively close to each other in time. This makes the Rx more tolerant towards the changes in the channel, extending its performance to support higher spreading factors, and at required SIR levels lower than the repetition technique. We can observe in Figure 4.9 that scrambling technique supports higher repetition factors compared to that of repetition technique, where the required SIR level using scrambling is reduced further than the breaking point of the repetition technique. This additional reduction in the required SIR is as much as 12 dB and 3 dB for the cases of 10% and 1% BERs respectively. Let us now study how the gain in the required SIR level (ΔSIR) achieved through scrambling translates to the improvement in the AmBCS coverage in the indoor, free-space, and outdoor environments.

Figure 4.10 shows the AmBCS coverage contour maps as a function of distances(in m), across different RF frequencies and propagation environments, for the breaking points of the Rx marked in the Figure 4.9 for repetition, and scrambling techniques. As we have already discussed the specific characteristics of AmBCS coverage for each propagation environment in the previous section, now we focus mainly on the increase in coverage due to scrambling, compared to the repetition technique. Let us start with the indoor environment.

In case of indoor environments, we can observe in Figure 4.10a that the coverage is considerably extended by implementing scrambling. This can be partially explained by the relatively low propagation exponent of indoor environments ($\eta = 1$), which has a gentle slope of path loss declined with distance. And due to this gentle slope, even the smaller difference in the SIR makes up for a bigger increase in the AmBCS coverage. It can be seen that the coverage in indoor environments is extended ≈ 4 times for the case of 10% BER, and ≈ 2 times for 1% BER, which is a significant improvement.

However, in case of free-space environment, as we can see in Figure 4.10b, the gain in coverage due to scrambling is ≈ 2.5 times for the case of 10% BER, and it is minimal for 1% BER case. Here, we can say that the benefit in coverage due to scrambling, is decreased when the propagation exponent increases. Let us study this behavior for an even higher propagation exponent, in the outdoor environment. Comparing Figure 4.10c across BERs, it can be seen that the gain in coverage due to scrambling is negligible in case of 1% BER compared to that of 10% BER. This can be partially explained by the relatively large propagation exponent of outdoor environments ($\eta = 4$), which has a greater slope of path loss declined with distance. And due to this greater slope, smaller increases in distance makes up for bigger differences in the changes of SIR. And, considering a nominal change of 3 dB in SIR, this explains the negligible coverage gain for 1% BER, compared to the 10% BER case which has an SIR gain of 12 dB.

Overall, it can be said that the improvement in coverage due to scrambling is comparatively more prominent for 10% BER across all RF frequencies and propagation environments. Moreover, the coverage areas for 1% BER is highly limited in the EPA channel and it can be seen in this Figure 4.10 that it is confined

to small regions surrounding the ambient RF source and the Rx. On the other hand, the results in Figure 4.10 shows that the scrambling technique has minimal influence on coverage in the outdoor propagation environment, but is useful for the case of the indoor environment.

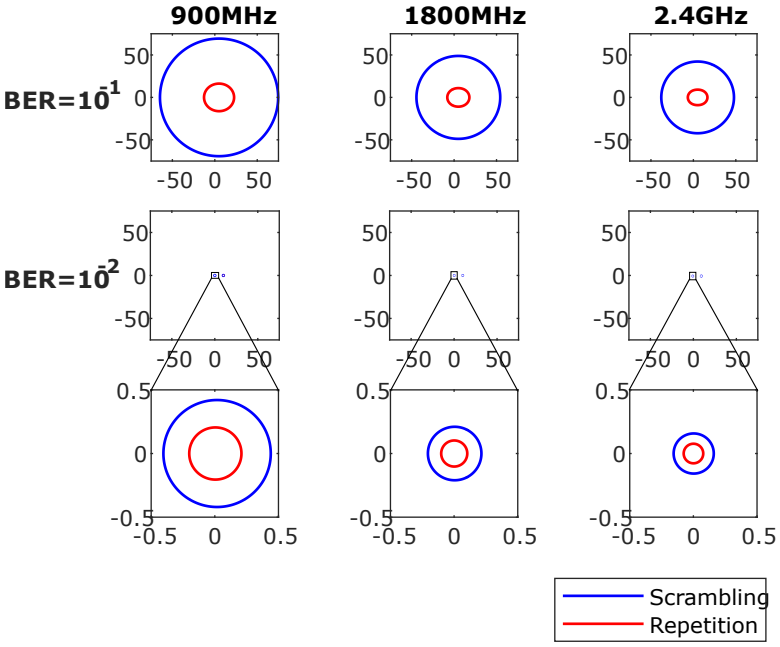

(a) Indoor environment ($\eta = 1$)

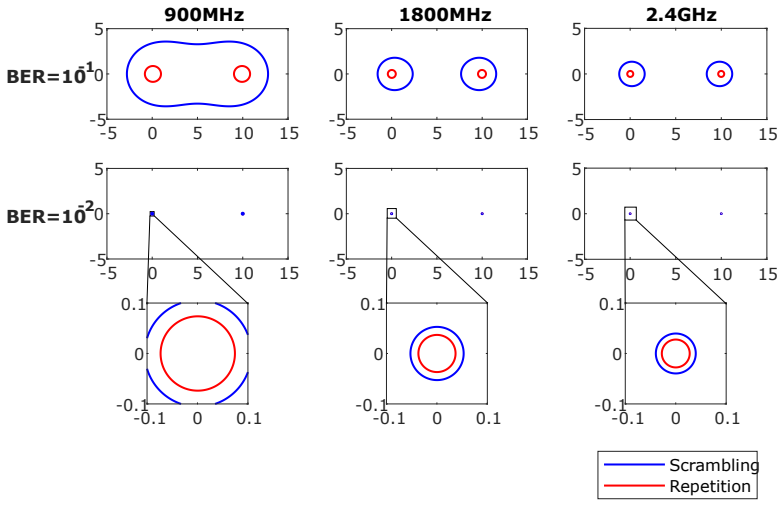

(b) Free space environment ($\eta = 2$)

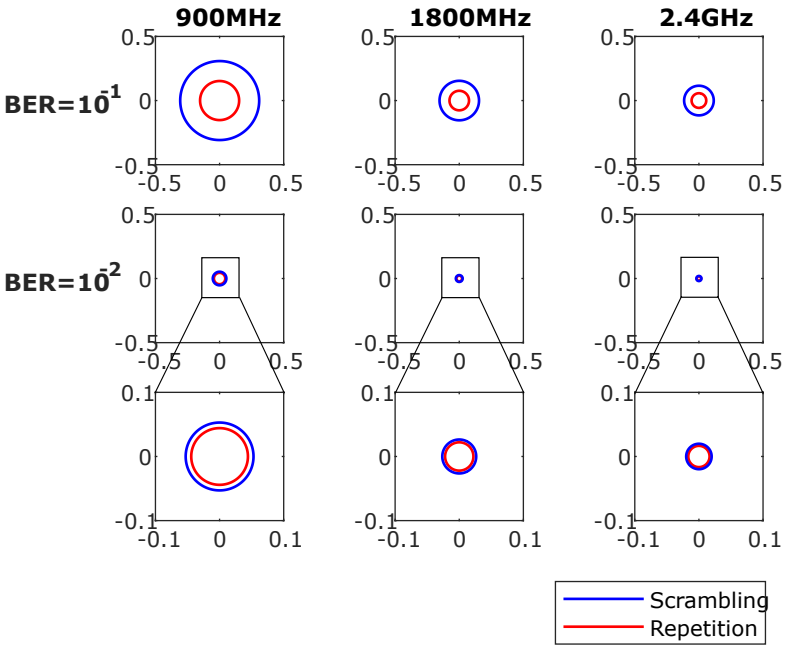

(c) Outdoor environment ($\eta = 4$)

Figure 4.10: Coverage comparison between repetition and scrambling techniques across the EPA channel for different BERs, and RF frequencies. Distances on x, and y axes in meters.

Chapter 5
Conclusion and Future Work

Ambient backscatter is an emerging wireless communication technology that has its prospects in a variety of small sensor type IoT applications. However, existing approaches in designing AmBCSs are based on extremely specific assumptions and it is relatively difficult to compare their performance capabilities. This makes it difficult to derive conclusions about the true potentials of AmBCSs from a general perspective. Therefore, in this work, we have discussed the relations among different performance metrics of AmBCSs using simple assumptions and simplified models.

In Chapter 2, we started with providing a general overview about the operation of different backscatter communication system types. Further, we have discussed various state-of-the-art designs and outlined the features and drawbacks of these designs. In Chapter 3, we discussed the analytical model of AmBCS along with the transmission scheme, detection scheme, and link budget in detail. Later in Chapter 4, we have presented our results, and discussed the AmBCS performance using different channel models, and propagation conditions. We have also discussed the relation between the performance metrics of AmBCSs. We then, studied the limitations of the chosen Rx structure in a realistic channel, and then discussed the prospects of using scrambling for making the Rx less susceptible to channel fading.

5.1 Conclusion

We have evaluated the influence of Rx noise on AmBCSs, and derived a condition for making AmBCSs into an interference-limited system, by analyzing the simulation results. This is done so that the performance of AmBCSs can be analyzed in a simplified manner. We have shown that the Rx noise can be safely ignored when the condition, INR $\geq$ 10 dB, is fulfilled. We have also discussed the reasons supporting that this aforementioned condition is a reasonable assumption in many realistic situations.

The characteristics of AmBCSs in most of the state-of-the-art studies are discussed only using performance metrics like data-rates and coverage. Despite being an important metric, analysis on BER is often not provided in these studies. In this work, we have discussed the relations among BER, data-rate, and coverage, under different propagation environments and RF frequencies, using simplified

channel models. We have shown that the AmBCS's data-rates should be reduced ≈ 100 times in order to meet a 1 order higher BER, while not losing any coverage. We have also studied the characteristics of AmBCS coverage across different propagation environments. It is also shown that AmBCSs are more suitable for indoor environments, and the coverage in outdoor environments can also be increased significantly, by carefully adapting the backscatter link environment.

However, the above analysis based on simplified channel assumption does not provide an accurate understanding about AmBCS performance in realistic scenarios. Therefore, we have also studied the AmBCS performance using the EPA channel model, which simulates more realistic and continuous fading. Here, we have shown the maximum limit for the repetition factor where the ML Rx structure starts failing due to continuous fading. We then compared the performance of repetition and scrambling techniques using the EPA channel and discussed the benefits of using scrambling. We have shown that the required SIR can be lowered as much as 12 dB and 3 dB for reaching BER requirements of 10% and 1%, respectively by using scrambling. The consequent improvement in the coverage due to scrambling is also discussed. In our coverage analysis for the EPA channel, we have shown that the benefits of scrambling in an outdoor environment can be negligible, but scrambling can support ≈ 4 times more coverage for 10% BER case, and ≈ 2 times more coverage for 1% BER case in an indoor environment.

To summarize, the major contributions of this thesis work are the conclusions drawn on the relations among the AmBCSs performance metrics and the effectiveness of scrambling in continuous fading channels. We have also analyzed the AmBCS coverage characteristics across various propagation environments. Another contribution is that we have addressed the problems of interference through the repetition technique, and channel fading through the scrambling technique, and provided a simple Rx structure for implementing the detection scheme for these two transmission techniques.

5.2 Future Work

This thesis work can be extended further in various directions. Some of the prospective additions that can be made to this work are listed below:

- Our work assumes perfect synchronization of the signal at the Rx. Further work is required to study the execution of this synchronization.
- The Rx is assumed to possess channel knowledge for correcting the errors due to phase rotation in the channel. Suitable approaches required for realizing this assumption without greatly increasing the complexity of the Rx need to be studied further.
- The AmBCS model discussed in this work is confined to a single backscatter device and the prospects of implementing multiple-access in AmBCSs can be studied further.
- Devices modeled in this work are assumed to have a single antenna at their terminals and the possibilities of improving backscatter performance using multiple antennas at the Rx can be an extension for this work.

- The raw BERs discussed in this work can be greatly improved by implementing error correcting codes at the backscatter device, which is another possible extension for this thesis.
- Energy harvesting techniques capable of generating the power required for backscatter devices using ambient RF signals should be investigated in order to realize AmBCSs as true zero-power communication systems.

References

[1] M. Lauridsen, R. Krigslund, M. Rohr and G. Madueno, "An Empirical NB-IoT Power Consumption Model for Battery Lifetime Estimation," 2018 IEEE 87th Vehicular Technology Conference (VTC Spring), 2018, pp. 1-5, doi: 10.1109/VTCSpring.2018.8417653.

[2] X. Li, N. Ma and P. Zhang, "Joint Pattern Assignment and Power Allocation for Energy Consumption Minimization for Massive MTC with PDMA," 2019 IEEE 5th International Conference on Computer and Communications (ICCC), 2019, pp. 1166-1171, doi: 10.1109/ICCC47050.2019.9064384.

[3] R. Ratasuk, N. Mangalvedhe, G. Lee and D. Bhatoolaul, "Reduced Capability Devices for 5G IoT," 2021 IEEE 32nd Annual International Symposium on Personal, Indoor and Mobile Radio Communications (PIMRC), 2021, pp. 1339-1344, doi: 10.1109/PIMRC50174.2021.9569595.

[4] D. Woods (2008). "Heliograph and Mirrors". In Sterling, Christopher (ed.). Military Communications: From Ancient Times to the 21st Century. ABC-CLIO. p. 208. ISBN 978-1851097326.

[5] P. V. Nikitin, K. V. S. Rao, S. F. Lam, V. Pillai, R. Martinez and H. Heinrich, "Power Reflection Coefficient Analysis for Complex Impedances in RFID Tag Design," in IEEE Transactions on Microwave Theory and Techniques, vol. 53, no. 9, pp. 2721-2725, Sept. 2005, doi: 10.1109/TMTT.2005.854191.

[6] G. Vannucci, A. Bletsas and D. Leigh, "A Software-Defined Radio System for Backscatter Sensor Networks," in IEEE Transactions on Wireless Communications, vol. 7, no. 6, pp. 2170-2179, June 2008, doi: 10.1109/TWC.2008.060796.

[7] J. Kimionis, A. Bletsas and J. N. Sahalos, "Bistatic Backscatter Radio for Power-limited Sensor Networks," 2013 IEEE Global Communications Conference (GLOBECOM), 2013, pp. 353-358, doi: 10.1109/GLOCOM.2013.6831096.

[8] J. D. Griffin and G. D. Durgin, "Complete Link Budgets for Backscatter-Radio and RFID Systems," in IEEE Antennas and Propagation Magazine, vol. 51, no. 2, pp. 11-25, April 2009, doi: 10.1109/MAP.2009.5162013.

[9] D. M. Dobkin, The RF in RFID: Passive UHF RFID in Practice.Newnes, NSW, Australia: Elsevier, 2008.

[10] H. Stockman, "Communication by Means of Reflected Power," in Proceedings of the IRE, vol. 36, no. 10, pp. 1196-1204, Oct. 1948, doi: 10.1109/JRPROC.1948.226245.

[11] K. Kurokawa, "Power Waves and the Scattering Matrix," in IEEE Transactions on Microwave Theory and Techniques, vol. 13, no. 2, pp. 194-202, March 1965, doi: 10.1109/TMTT.1965.1125964.

[12] V. Talla and J. R. Smith, "Hybrid Analog-Digital Backscatter: A New Approach for Battery-Free Sensing," 2013 IEEE International Conference on RFID (RFID), 2013, pp. 74-81, doi: 10.1109/RFID.2013.6548138.

[13] J. Kimionis, A. Bletsas and J. N. Sahalos, "Increased Range Bistatic Scatter Radio," in IEEE Transactions on Communications, vol. 62, no. 3, pp. 1091-1104, March 2014, doi: 10.1109/TCOMM.2014.020314.130559.

[14] S. H. Choi and D. I. Kim, "Backscatter Radio Communication for Wireless Powered Communication Networks," 2015 21st Asia-Pacific Conference on Communications (APCC), 2015, pp. 370-374, doi: 10.1109/APCC.2015.7412542.

[15] X. Lu, D. Niyato, H. Jiang, D. I. Kim, Y. Xiao and Z. Han, "Ambient Backscatter Assisted Wireless Powered Communications," in IEEE Wireless Communications, vol. 25, no. 2, pp. 170-177, April 2018, doi: 10.1109/MWC.2017.1600398.

[16] V. Talla, M. Hessar, B. Kellogg, A. Najafi, J. R. Smith and S. Gollakota, “LoRa Backscatter: Enabling The Vision of Ubiquitous Connectivity,” in arXiv: Networking and Internet Architecture, September 2017, doi: 10.1145/3130970

[17] A. Varshney, O. Harms, C. Pérez-Penichet, C. Rohner, F. Hermans and T. Voigt, "LoRea: A Backscatter Architecture That Achieves a Long Communication Range", in Proceedings of the 15th ACM Conference on Embedded Network Sensor Systems, 2017, doi: 10.1145/3131672.3131691.

[18] V. Liu, A. Parks, V. Talla, S. Gollakota, D. Wetherall and J. R. Smith, "Ambient Backscatter: Wireless Communication out of Thin Air", in Proceedings of the ACM SIGCOMM 2013 Conference on SIGCOMM, 2013, pp. 39–50, doi: 10.1145/2534169.2486015.

[19] A. N. Parks, A. Liu, S. Gollakota and J. R. Smith, "Turbocharging Ambient Backscatter Communication", in Proceedings of the 2014 ACM Conference on SIGCOMM, 2014, pp. 619–630, doi: 10.1145/2740070.2626312.

[20] A. Wang, V. Iyer, V. Talla, J. R. Smith and S. Gollakota, "FM Backscatter: Enabling Connected Cities and Smart Fabrics", in 14th USENIX Symposium on Networked Systems Design and Implementation (NSDI 17), 2017, pp. 243–258.

[21] B. Kellogg, A. Parks, S. Gollakota, J. R. Smith and D. Wetherall, "Wi-Fi Backscatter: Internet Connectivity for RF-Powered Devices", in Proceedings of the 2014 ACM Conference on SIGCOMM, 2014, pp. 607–618 doi: 10.1145/2619239.2626319.

[22] P. Zhang, D. Bharadia, K. Joshi and S. Katti, "HitchHike: Practical Backscatter Using Commodity WiFi", in Proceedings of the 14th ACM Conference on Embedded Network Sensor Systems CD-ROM, 2016, pp. 259–271, doi: 10.1145/2994551.2994565.

[23] B. Kellogg, V. Talla, S. Gollakota and J. R. Smith, "Passive Wi-Fi: Bringing Low Power to Wi-Fi Transmissions", in 13th USENIX Symposium on Networked Systems Design and Implementation (NSDI 16), 2016, pp. 151–164.

[24] D. Bharadia, K. R. Joshi, M. Kotaru and S. Katti, "BackFi: High Throughput WiFi Backscatter", in Proceedings of the 2015 ACM Conference on Special Interest Group on Data Communication, 2015, pp. 283–296, doi: 10.1145/2829988.2787490.

[25] V. Iyer, V. Talla, B. Kellogg, S. Gollakota and J. Smith, "Inter-Technology Backscatter: Towards Internet Connectivity for Implanted Devices", in Proceedings of the 2016 ACM SIGCOMM Conference, pp. 356–369, doi: 10.1145/2934872.2934894.

[26] P. Zhang, M. Rostami, P. Hu and D. Ganesan, "Enabling Practical Backscatter Communication for On-Body Sensors", in Proceedings of the 2016 ACM SIGCOMM Conference, pp. 370–383, doi: 10.1145/2934872.2934901.

[27] N. Van Huynh, D. T. Hoang, X. Lu, D. Niyato, P. Wang and D. I. Kim, "Ambient Backscatter Communications: A Contemporary Survey," in IEEE Communications Surveys and Tutorials, vol. 20, no. 4, pp. 2889-2922, Fourthquarter 2018, doi: 10.1109/COMST.2018.2841964.

[28] C. Xu, L. Yang and P. Zhang, "Practical Backscatter Communication Systems for Battery-Free Internet of Things: A Tutorial and Survey of Recent Research," in IEEE Signal Processing Magazine, vol. 35, no. 5, pp. 16-27, Sept. 2018, doi: 10.1109/MSP.2018.2848361.

[29] 3GPP TS 36.101 "User Equipment (UE) radio transmission and reception".

[30] "LteFadingChannel," Propagation Channel Models- MATLAB & amp; Simulink - MathWorks Nordic, https://se.mathworks.com/help/lte/ug/propagation-channel-models.html.

[31] Daeyoung Kim, M. A. Ingram and W. W. Smith, "Measurements of Small-Scale Fading and Path Loss for Long Range RF Tags," in IEEE Transactions on Antennas and Propagation, vol. 51, no. 8, pp. 1740-1749, Aug. 2003, doi: 10.1109/TAP.2003.814752.

[32] S. J. Thomas and M. S. Reynolds, "A 96 Mbit/sec, 15.5 pJ/bit 16-QAM Modulator for UHF Backscatter Communication," 2012 IEEE International Conference on RFID (RFID), 2012, pp. 185-190, doi: 10.1109/RFID.2012.6193049.

[33] A. Shirane et al., "RF-Powered Transceiver With an Energy- and Spectral-Efficient IF-Based Quadrature Backscattering Transmitter," in IEEE Journal of Solid-State Circuits, vol. 50, no. 12, pp. 2975-2987, Dec. 2015, doi: 10.1109/JSSC.2015.2454235.

[34] K. Lu, G. Wang, F. Qu and Z. Zhong, "Signal detection and BER analysis for RF-powered devices utilizing ambient backscatter," 2015 International Conference on Wireless Communications & Signal Processing (WCSP), 2015, pp. 1-5, doi: 10.1109/WCSP.2015.7341107.

[35] J. Qian, F. Gao, G. Wang, S. Jin and H. Zhu, "Semi-Coherent Detection and Performance Analysis for Ambient Backscatter System," in IEEE Transactions on Communications, vol. 65, no. 12, pp. 5266-5279, Dec. 2017, doi: 10.1109/TCOMM.2017.2738001.

[36] Y. Liu, G. Wang, Z. Dou and Z. Zhong, "Coding and Detection Schemes for Ambient Backscatter Communication Systems," in IEEE Access, vol. 5, pp. 4947-4953, 2017, doi: 10.1109/ACCESS.2017.2679135.

Printed by Tryckeriet i E-huset, Lund 2022

LUND
UNIVERSITY

Series of Master's theses
Department of Electrical and Information Technology
LU/LTH-EIT 2022-894
http://www.eit.lth.se